Title: Pervasive iron limitation at subsurface chlorophyll maxima of the California Current

Authors: Shane L. Hogle[1]*, Chris L. Dupont[2], Brian Hopkinson[3], Andrew L. King[4], Kristen N. Buck[5], Kelly L. Roe[6], Rhona K. Stuart[1,7], Andrew E. Allen[1,2], Elizabeth L. Mann[8], Zackary I. Johnson[9], Katherine A. Barbeau[1]

[1]Scripps Institution of Oceanography, La Jolla, California, USA

[2]J. Craig Venter Institute, La Jolla, California, USA

[3]Department of Marine Sciences, University of Georgia, Athens, GA, USA

[4]Norwegian Institute for Water Research, Bergen, Norway

[5]College of Marine Science, University of South Florida, St. Petersburg, FL, USA

[6]Finger Lakes Community College, Canandaigua NY, USA

[7]Lawrence Livermore National Laboratory, Livermore, CA, USA

[8]Bigelow Laboratory for Ocean Sciences, East Boothbay ME, USA

[9]Nicholas School of the Environment and Biology Department, Duke University Marine Laboratory, Beaufort, NC, USA

Corresponding author email: S.L.H (shogle@mit.edu) or K.A.B (kbarbeau@ucsd.edu)

*Present Address: Shane L. Hogle, Department of Civil and Environmental Engineering, Massachusetts Institute of Technology, Cambridge, Massachusetts, USA.

Introductory paragraph/abstract: Subsurface chlorophyll maximum layers (SCMLs) are nearly ubiquitous in stratified water columns and exist at horizontal scales ranging from the submesoscale to the extent of oligotrophic gyres. These layers of heightened chlorophyll and/or phytoplankton concentrations are generally thought to be a consequence of a balance between

light energy from above and a limiting nutrient flux from below, typically nitrate. Here we present multiple lines of evidence demonstrating that iron (Fe) limits or with light co-limits phytoplankton communities in SCMLs along a primary productivity gradient from coastal to oligotrophic offshore waters in the southern California Current ecosystem. SCML phytoplankton responded markedly to added Fe or Fe/light in experimental incubations, biogeochemical proxies for Fe limitation peaked in SCML waters, and transcripts of diatom and picoeukaryote Fe stress genes were strikingly abundant in SCML metatranscriptomes. A 40-year time-series indicates that SCMLs in this region display a persistent biogeochemical signal of diatom Fe deficiency during the spring and summer months, particularly within inshore and transition zones. In addition, the spatial extent of SCML Fe limitation has markedly increased during the first decade of the 21st century. We conclude that phytoplankton Fe limitation and Fe/light co-limitation at SCMLs is an important constraint on primary productivity and carbon export in the California Current and potentially SCMLs worldwide.

Fe and light are essential for phytoplankton photosynthesis, but both resources are scarce in much of the ocean. Marine primary productivity may be limited by the availability of Fe in 40% of the surface ocean[1], and mesoscale Fe fertilization experiments now firmly demonstrate that Fe availability controls phytoplankton biomass and growth rates in the Southern, equatorial Pacific, and subarctic Pacific oceans[2]. In addition, phytoplankton Fe limitation has been observed in mid-latitude coastal upwelling zones[3,4], throughout mesoscale circulation features[5], and at the edge of subtropical gyres[6]. In the surface ocean light attenuates rapidly to less than 1% of incident photosynthetically available radiation ($z_{1\%}$) at depths from 50-200 meters depending on turbidity. However, many diverse phytoplankton groups have adapted to growth at depths approaching $z_{1\%}$ despite the challenging low-light conditions. Prior studies noting the overlapping scarcity of Fe and light in much of the ocean predicted that these two resources synergistically co-limit phytoplankton growth[7,8], particularly in SCMLs[9]. Indeed, work with

53 cultured phytoplankton demonstrates that Fe/light co-limitation can arise when demand for Fe-
54 rich photosynthetic redox proteins increase under low light conditions[9–11]. However, the potential
55 for phytoplankton Fe or Fe/light (co-)limitation in SCMLs has only been explored in a handful of
56 field studies despite the significant feedbacks linking (co-)limitation, dust deposition, and
57 oceanic CO_2 uptake in global biogeochemical models[12]. Although Fe/light co-limitation has been
58 observed in some high-latitude SCMLs[13,14], mid/low latitude SCMLs from both coastal and
59 pelagic zones remain understudied. Dissolved Fe minima at SCMLs from the subtropical North
60 Pacific gyre[15] and the Sargasso Sea[16] may be a consequence of intense biological demand,
61 even Fe limitation, during summer months. One study documented phytoplankton Fe/light co-
62 limitation from mesotrophic and oligotrophic SCMLs in the California Bight and the eastern
63 tropical North Pacific[17], while another found SCMLs in the oligotrophic Western Pacific to be
64 mostly light limited with some groups of microbial eukaryotes potentially exhibiting Fe/light co-
65 limitation[18]. However, studies employing multiple complementing experimental approaches at
66 varied scales are needed to establish the prevalence of phytoplankton Fe limitation or Fe/light
67 co-limitation within SCMLs worldwide.
68
69 **Oceanographic setting:** High productivity in the southern California Current (CC) and other
70 Eastern Boundary Current systems is supported by intense upwelling of macronutrient rich
71 waters[19]. However, local variation in Fe concentrations and other biogeochemical factors can
72 generate Fe limited phytoplankton communities in the CC[4,5,20]. During July 2007 we investigated
73 the role of Fe and light as (co-)limiting factors along a transect of CalCOFI Line 93.3, which
74 spans the Inshore (approximately 0-150 km offshore), Transition (approximately 150-450 km
75 offshore), and Offshore (approximately 450 km offshore) zones of the southern CC. In addition
76 to sampling all standard CalCOFI stations on this transect, we intensively sampled three
77 stations (93.3/40, 93.3/80, and 93.3/120) representing the Inshore, Transition, and Offshore
78 zones respectively[21,22]. At these three stations we measured total dissolved Fe (dFe)

concentrations and the concentrations of strong, organic Fe-binding ligands (L_1). L_1 concentrations are positively correlated with Fe-limited phytoplankton growth in incubation studies, suggesting that phytoplankton and/or associated bacteria may actively produce L_1 as an adaptation to Fe limitation[23–26]. We also determined two other biogeochemical proxies for Fe limitation: the NO_3 to dFe ratio (N:dFe) and Si_{ex}. Briefly, when N:dFe is at or above 8 (μmol/nmol) phytoplankton reliably respond to added Fe by increasing nitrate consumption, cellular chlorophyll *a*, and total cell numbers[4,27]. Si_{ex} is a modified form of the Si* proxy[28] and traces shifts in the elemental composition of diatoms as a result of Fe-limitation[29] (see supplementary text for further discussion). Negative Si_{ex} values in the water column indicate preferential diatom uptake of Si relative to NO_3 due to Fe limitation. Si_{ex} and the N:dFe ratio were negatively correlated across all samples ($\rho = -0.75$, $P = 2.4e^{-7}$) indicating that low Si and high NO_3 waters generally also had low Fe concentrations, consistent with Fe limiting conditions for diatoms (Supplementary Fig. 1).

At each of the intensively sampled stations we conducted incubation experiments with factorial resource additions of Fe, light, and combined Fe+light to SCML water. We measured chlorophyll *a* concentrations, primary production rates, the photochemical quantum efficiency of PSII (Fv/Fm), nitrate consumption over the course of the incubations, and phytoplankton community composition by microscopy. Using these measurements we then classified incubation responses as either simultaneous co-limitation, independent co-limitation, or serial limitation[30] (see supplemental text for definitions of limitation and stress). Community transcriptomes were collected and sequenced from SCML and surface waters (Fig. 1A,B) and were introduced in a prior publication[31]. Here we focus on expression patterns of phytotransferrin (pTF), formerly known as ISIP2A[32], and of Iron Stress Inducible Protein 3 (ISIP3), which are diagnostic biosignatures of algal Fe limitation in culture[32–34] and in the field[35–37].

Fe limitation at SCMLs of the Inshore CC sector: Biogeochemical proxies (Si_{ex} and N:dFe ratio), community transcriptomes, and incubation experiments consistently pointed to significant diatom Fe limitation at Inshore SCMLs and were indicative of serial or single Fe limitation rather than co-limitation[30]. Fe concentrations were low in the surface mixed layer (mean of 0.10 nmol L^{-1}) and the depths of the ferricline (74 m) and nitracline (31 m) were strongly decoupled at station 93.3 / 40 (Fig. 1C, Supplementary Table 1). L_1 concentrations peaked at the SCML, N:dFe ratios were strikingly elevated ($N:dFe_{max}$ = 120 µmol/nmol) within the SCML, and the Si_{ex} profile mirrored that of N:dFe (Fig. 1C). The SCML incubation experiments displayed a nearly 5-fold increase in total chlorophyll *a*, bulk nitrate consumption, and quantum efficiency in response to added Fe and Fe+light but not to light alone or control conditions (Fig. 2). Primary production rates increased the most with added Fe+light and Fe, while light alone had no effect. Large chain forming diatoms dominated in added Fe and Fe+light incubation conditions (Supplementary Fig. 2). ISIP3 and pTF transcripts were strikingly abundant in community transcriptomes from the SCML at station 93.3/40 with transcripts from four taxonomic groups exceeding the 95th rank percentile of all annotated community transcripts (Fig. 3). *Phaeocystis* and *Pelagomonas* pTFs were the most abundant and exceeded the 99th rank abundance percentile of all community transcripts. The expression of pTF/ISIP3 by Diatoms, *Pelagomonas*, and *Phaeocystis* often equalled or exceeded that of highly-expressed genes for essential cellular functions from each taxonomic group including ribosomal assembly proteins, heat shock-like proteins, and photosynthesis-related proteins (Supplementary Fig. 3). Proteorhodopsin-like genes, which have recently been proposed as an alternative, Fe-independent energy acquisition strategy for iron-limited diatoms[38], were some of the most highly expressed diatom transcripts at the SCML of 93.3/40 - perhaps also due to Fe limitation.

Fe/light co-limitation at the CC Transition and Offshore zones: At the oligotrophic edge of the Transition zone and in the Offshore zone we observed a deepening of the nitracline and SCML towards the base of the euphotic zone where low light levels may have increased photosynthetic Fe demand to the point of Fe/light co-limitation. SCMLs at stations 93.3/80 and 93.3/120 displayed multiple signatures of potential Fe/light co-limitation. dFe concentrations were again low in the surface mixed layer (mean of 0.13 and 0.11 nmol L^{-1} in the transition and offshore zones, respectively) and the depths of the ferricline and nitracline were strongly decoupled at station 93.3/120 and moderately offset at station 93.3/80 (Fig. 1 C). We observed a localized Fe depletion at the outer Transition zone SCML, potentially due to enhanced localized biological Fe uptake. We also measured a localized L_1 increase at the Offshore zone SCML, consistent with enhanced biological production of Fe acquisition molecules at this depth. N:dFe ratios greater than 8 µmol/nmol and negative Si_{ex} values highlighted the base of the SCML as a region of potential diatom Fe limitation in most of the Transition zone. In the Offshore zone, negative Si_{ex} tracked the σ_θ = 26 kg m^{-3} isopycnal to depths 100 m below the euphotic zone, indicating that the signal may not have been from local diatom Fe limitation and potentially Fe-limited waters advected from elsewhere (see supplemental text). In this sector mesoscale circulation features[20,39] and wind stress curl upwelling[40] are likely important sources of new N to the euphotic zone, but may be too infrequent to generate chronic Fe-limited diatom growth and a persistent Si_{ex} signal at the SCML.

In incubation experiments from the outer Transition zone and Offshore SCMLs we observed a roughly 2-fold increase in diatom growth (Supplementary Fig. 2), nitrate drawdown, and increased photosynthetic efficiency in response to added Fe+light consistent with Fe/light co-limitation scenarios. The outer Transition zone responses were most consistent with independent Fe/light co-limitation (see limitation definitions in supplemental text). Fe+light stimulated the greatest nitrate drawdown, primary production, and total chlorophyll *a* increases,

while responses to Fe or light alone were diminished. However, the separate addition of both iron and light significantly enhanced nitrate drawdown and the addition of iron increased the chlorophyll *a* concentration. In contrast, offshore incubation responses were similar to those from the Transition zone but potentially reflected a simultaneous co-limitation scenario whereby only Fe+Light produced a significant increase in chlorophyll *a*, primary production, and nitrate consumption. Although smaller non-chain forming diatoms were the dominant responders to the Offshore zone Fe addition incubations (Supplementary Fig. 2), the *in situ* positive Si_{ex} signal at the Offshore SCML suggests that Fe-limited diatoms were not abundant at the time of sampling. Indeed, *Pelagomonas*, *Phaeocystis*, and *Dinophyceae* ptF/ISIP3 transcripts exceeded the 99th rank abundance percentile for all community transcripts in the Offshore and Transition zones SCMLs (Fig. 3) and were comparable in abundance to highly-expressed genes from major metabolic pathways (Supplementary Fig. 3). These patterns suggest that small non-silicifying phytoplankton in the Transition and Offshore zones were investing significant resources into Fe acquisition.

Fe limitation at SCMLs of the CC estimated from a 40-year time series: We sought to characterize the potential for Fe limitation in the southern CC across broader spatial and temporal scales by leveraging 40 years of monthly sampling data collected from 75 stations distributed over a 190,000 km^2 area as a part of the CalCOFI program (http://calcofi.org/). We used Si_{ex} as a biogeochemical proxy for diatom Fe limitation because Si and NO_3 measurements are readily available in the CalCOFI dataset and there is a strong correlation between negative Si_{ex} and experimentally determined Fe limitation in our results and the results of others[5,20,29]. Although Si_{ex} is potentially sensitive to mixing/advection, shifts in upwelling source depth, and other processes that may integrate nonspecific biogeochemical signals, we argue that the effect of these processes are likely be minimal in the southern CC and that Si_{ex} is a robust indicator for diatom Fe limitation effects (see supplementary text).

During the spring and summer months over the last 40 years approximately 30% of all SCML samples in the southern CC displayed a negative Si_{ex} signal. This signal is disproportionately concentrated in SCMLs from the Inshore (43% negative) and Transition zone (26% negative) compared with the Offshore (7% negative) (Fig 4, Supplementary Fig. 4). On average Si_{ex} from Inshore and Transition zone SCMLs has steadily become more negative since 2000 in contrast to the general increase of the 1990s and most of the 1980s (Supplementary Fig. 5). We also find that the total spatial range of SCMLs with negative Si_{ex} values has significantly increased for the Inshore sector over the last 40 years (Fig 4E). These trends have occurred in conjunction with a general shoaling of the SCML, nitracline, and euphotic zone in the southern CC (Supplementary Fig. 6)[21,40,41], particularly for the Offshore and Transition zones during the early 2000s. Negative Si_{ex} values often coincided with the highest observed chlorophyll *a* concentrations in the Inshore zone (Supplementary Fig. 4) suggesting a major contribution of Fe limited diatoms to coastal primary production. Negative Si_{ex} values in the Offshore zone generally tracked the base of the euphotic zone (Supplementary Fig. 7) or extended below it (Fig. 1A). This signal may be caused by chronic *in situ* diatom Fe limitation at the deepest parts of the Offshore euphotic zone and/or may reflect along-isopycnal propagation of a negative Si_{ex} signal generated inshore as has been observed for other tracers[42,43].

Patterns of Negative Si_{ex}, CC winds, the NPGO, and biogeochemical variables: Negative Si_{ex} at the SCML may track decadal modes of climate variability in the southern CC. The North Pacific Gyre Oscillation (NPGO) mode is a large-scale climatological index that is significantly correlated with fluctuations in the biogeochemistry and hydrography of the southern CC[44]. Positive NPGO intervals (Supplementary Fig. 8) are associated with wind shifts that result in upwelling-favorable conditions in the CC[44] and coincide with the most extreme negative Si_{ex} events from the last 40 years (Supplementary Fig. 5). The strengthening of the NPGO amplitude

since 1993[44] also corresponds with an increase in the Inshore spatial extent of diatom Fe limitation at the SCML (Fig. 4F), potentially indicating shared forcing. However, the time-lagged correlations between Si_{ex} extent and wind-stress curl or Ekman driven coastal upwelling are quantitatively weak ($\rho < 0.2$, Supplementary Fig. 9). This apparent weak correlation may actually reflect nonlinear[45] or cumulatively integrative[46] responses and does not necessarily exclude a mechanistic relationship between regional Si_{ex} trends at the SCML and decadal patterns of atmospheric forcing. Further study is needed to uncover the mechanisms potentially driving the negative Si_{ex} signal.

Si_{ex} signals at the SCML were strongly negatively correlated with SCML nitrate concentrations ($\rho = -0.77$, $P < 1e^{-200}$) and more moderately correlated with the difference between the nitracline and SCML depths ($\rho = 0.53$, $P < 1e^{-200}$) and the potential density at the SCML ($\rho = -0.49$, $P < 1e^{-200}$) (Supplementary Fig. 9). The tight negative correlation between SCML nitrate concentrations and Si_{ex} is consistent with diatom Fe (co-)limitation preventing complete nitrate drawdown at the SCML, and the positive correlation with nitracline/SCML depth offset similarly suggests that diatom Fe limitation emerges when SCMLs form below the top of the nitracline in higher nitrate waters. The correlation between Si_{ex} and SCML potential density may reflect an association with Fe limitation and increased isopycnal shoaling or increasing upwelling strength in general.

Conclusions: The diagnosis of nutrient limitation *in situ* is a critical step towards better understanding fluxes of energy and matter in marine ecosystems. Our results suggest a strong coastal to offshore gradient in the combined effects of iron and light on SCML phytoplankton of the southern CC, a highly productive eastern boundary upwelling regime. The shallower Inshore and inner Transition zone SCML communities, which represent maxima in both diatom biomass and productivity, appear particularly susceptible to single or serial Fe limitation, while deeper

SCML communities from the outer Transition and oligotrophic Offshore zones may experience periods of Fe/light co-limitation or oscillate between Fe, macronutrient, or light single limitation. Historical inferred patterns of diatom iron deficiency in the CC appear to track dominant modes of climate variability in the North Pacific, which may be due to regional atmospheric patterns that decouple the nitracline, ferricline, and the SCML. This potential atmospheric-biogeochemical linkage provides a new connection, mediated by iron, by which climate change may influence carbon cycling and primary productivity in the California Current and potentially other eastern boundary currents. Biogeochemical models predict increased upwelling and nitrate fluxes to the southern California Current under anthropogenic climate change[47,48], which may drive diatom communities at the SCML towards Fe limitation if associated Fe fluxes do not increase proportionally. Diatom Fe (co-)limitation at SCMLs and the resulting increased silicification may also enhance particulate carbon export efficiency by increasing sinking rates and shielding cells from grazing[5,20]. Fe limitation and Fe/light co-limitation at SCMLs needs to be recognized as a potentially significant force shaping new production and carbon cycling in the CC, other productive eastern boundary systems, and potentially the oligotrophic ocean.

Acknowledgements: We thank the captain and crew of the *RV New Horizon*. We express our gratitude to all past and present members of the CalCOFI program for generating a comprehensive, high quality data set and for making this data freely available and easily accessible. We thank Melissa Carter for phytoplankton cell counts and the staff at JCVI for assistance with sequencing. Field work was funded by NSF grant OCE-0550302 to KAB and EM and NSF grant 05-507098 to ZJ. KAB acknowledges additional support from the California Current Ecosystem Long Term Ecological Research Program (LTER NSF/OCE-0417616 and OCE-1026607). Metatranscriptomes are derived from the Global Ocean Sampling expedition and were funded through JCVI internal funds and the US Department of Energy, Office of Science, Office of Biological and Environmental Research (DE-FC02-02ER63453). A portion of

this work was performed under the auspices of the U.S. Department of Energy by Lawrence Livermore National Laboratory under Contract DE-AC52-07NA27344.

Author contributions: KAB, EM, and ZJ conceived of and initiated the project. SLH contributed new hypotheses and research directions, analyzed metatranscriptomes and metagenomes, processed incubation data, processed biogeochemical measurements, and analyzed archival CalCOFI data. SLH wrote all code and performed all statistical analyses. SLH and KAB wrote the paper with participation of BMH, ALK, KNB, CLD, ZJ, EM, AEA, RKS, and KLR. BMH, KLR, and KAB conducted incubation experiments. ALK measured dissolved Fe concentrations. KNB measured Fe-binding ligand concentrations. RKS and CLD collected metagenomes and metatranscriptomes. AEA and CLD sequenced, processed, and annotated metagenomes and metatranscriptomes. ZJ measured photosynthetic efficiency and primary production. All authors were involved in the discussions of the results and commented on the manuscript.

Competing financial interests: The authors declare no competing financial interests.

Correspondence: Address correspondence to SLH (shogle@mit.edu) or KAB (kbarbeau@ucsd.edu).

Materials & Data Availability: All data supporting the findings of this study are available the following websites. CalCOFI time series data are available from the CalCOFI data archives (http://new.data.calcofi.org/index.php/reporteddata). Metatranscriptome and metagenome biological sequence files are available from iMicrobe (https://imicrobe.us, iMicrobe project ID: CAM_P_0001069). Biogeochemical data subsets, metatranscriptome annotations, and all computer code required to reproduce the results reported in this study are available from Figshare (https://doi.org/10.6084/m9.figshare.6033761.v1) and Github

(https://github.com/slhogle/DCM2007). Unprocessed biogeochemical data are available from the UCSD Datazoo Research Project (http://oceaninformatics.ucsd.edu/datazoo/catalogs/ccelter/sources/1758).

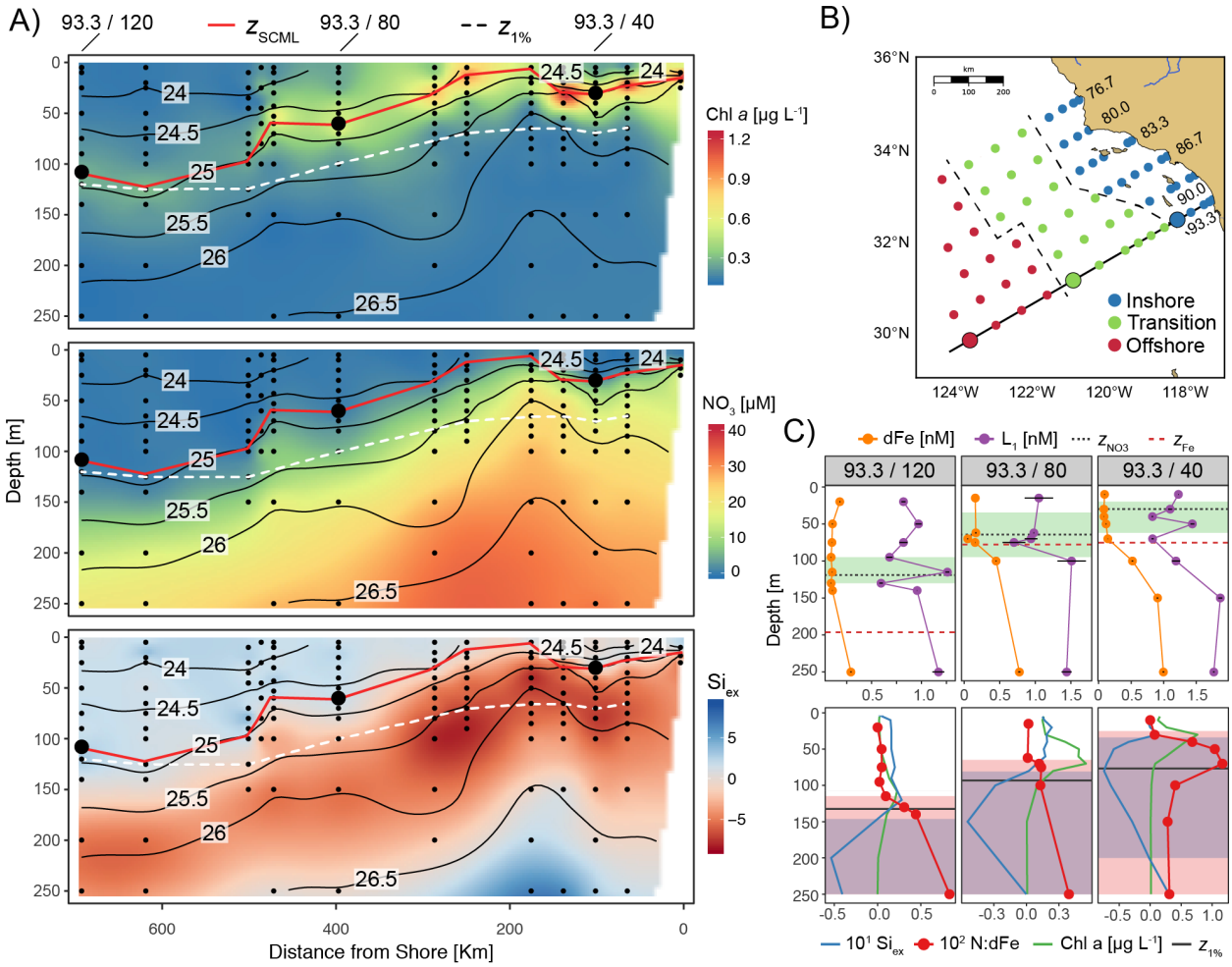

Fig 1: A) Section plots of Chl *a* (top), nitrate (middle), and Si_{ex} determined using $R_{Si:N}$ from σ_θ = 26.5 kg m^{-3} (bottom) along CalCOFI line 93.3 sampled during the July 2007 cruise. Numeric labels denote values for potential density anomaly (σ_θ kg m^{-3}) contours. Small circles denote nutrient/hydrographic sampling depths and large circles represent SCML sampling depths used for incubations and metatranscriptomics. The white and red dashed lines represent the depth of 1% of incident irradiance ($z_{1\%}$) and SCML depth (z_{SCML}), respectively. B) CalCOFI sampling grid labeled by line number. The three SCML locations sampled for incubations and metatranscriptomics are shown as large circles. C) (Top half) Profile plots of dissolved Fe concentrations (orange) and L_1 concentrations (purple). The green box denotes depths where Chl *a* is within 50% of z_{SCML} concentration, the dashed black line is nitracline depth (z_{NO3}), and the dashed red line is ferricline depth (z_{Fe}). L_1 and dFe error bars represent standard deviations of triplicate replicates for each measurement. (Bottom half). Profiles of Chl *a* (green), 10x Si_{ex} (blue), and 10^2 x N:dFe ratio (red circle). The black line represents the $z_{1\%}$ depth. Red (N:dFe > 8) and blue (Si_{ex} < 0) regions represent depth strata where each proxy has exceeded threshold values typical for diatom Fe limitation. Purple regions represent depths where both Si_{ex} and N:dFe indicate potential for Fe limitation.

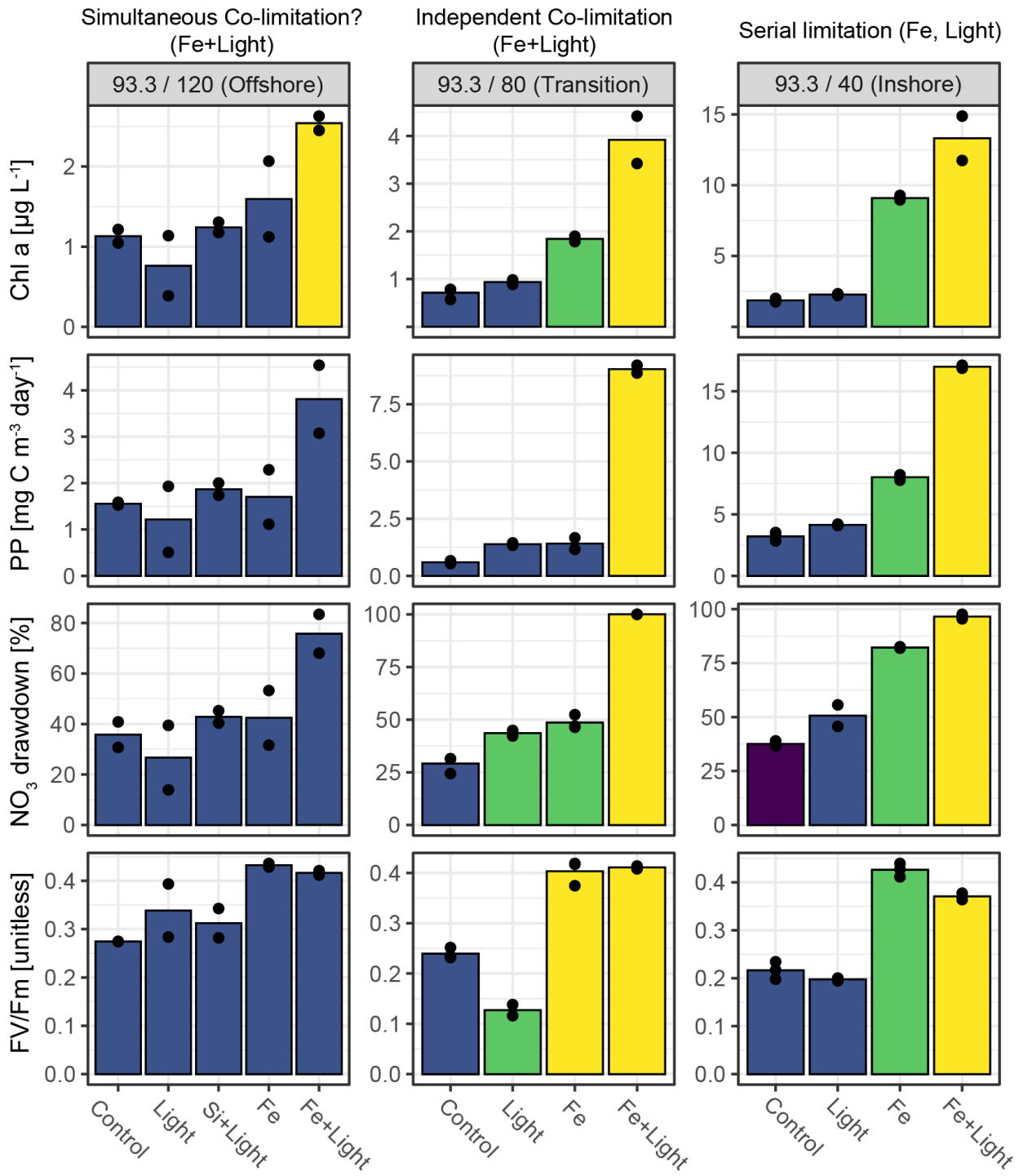

Fig. 2: Chlorophyll *a* concentrations, Primary production, maximum quantum yield of photosystem II, and nitrate drawdown from the final time point of incubation experiments conducted at stations 93.3/40, 93.3/80, and 93.3/120 during the DCM07 cruise. Bars represent means of replicate incubations (individual dots). Conditions with statistically different group means in each experiment are colored separately (ANOVA and pairwise t-test with false discovery rate corrected $P \leq 0.05$). At 93.3 / 120 we included a silicate+light incubation treatment in order to test for potential diatom silicate limitation (not observed). The most parsimonious mode of nutrient limitation is listed above each station (see supplementary text for definitions). Note vertical axis scales for each station are different.

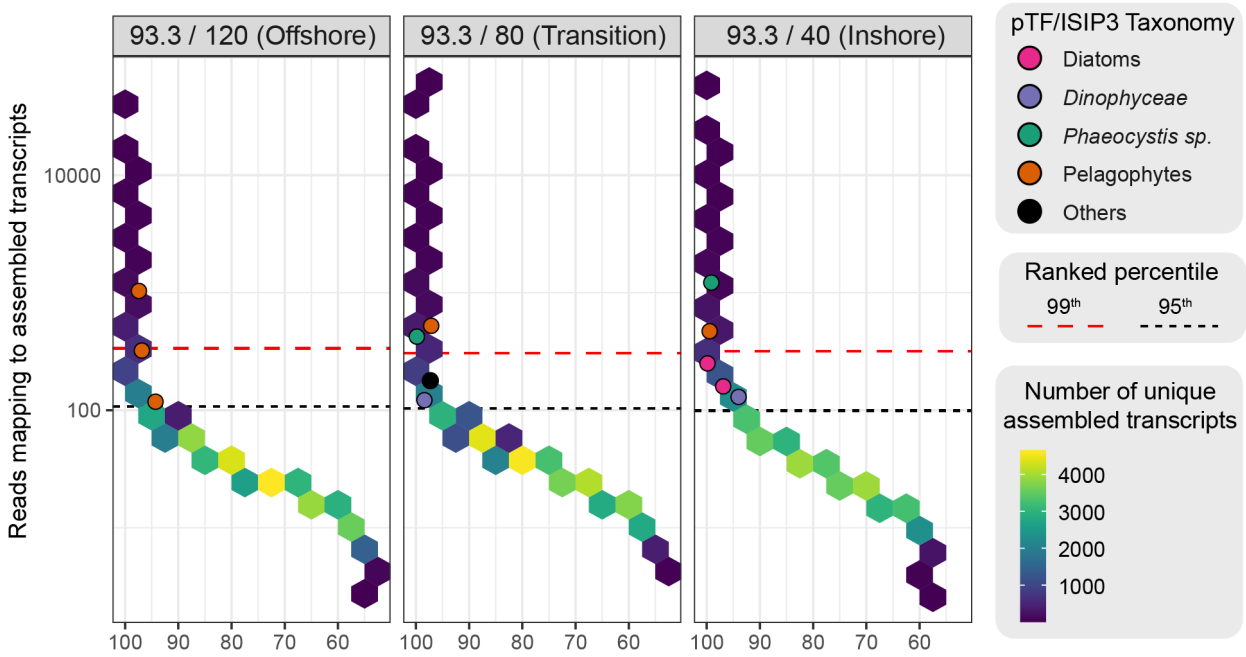

Fig. 3: Rank abundance plots for assembled transcripts from each SCML metatranscriptome sample. Position on the vertical axis (log_{10} scale) depicts the reads per kilobase of transcript per million mapped reads (RPKM) and horizontal axis equals the windowed percentile transcript ranking per metatranscriptome. Each hexagonal bin depicts a spatial histogram on the RPKM vs Rank abundance grid and the color of each bin is proportional to the number of binned transcripts within that gridded area. Individual pTF/ISIP3 transcripts at or above the 95th percentile ranking in each metatranscriptome are denoted by points and are colored according to their taxonomic classification. Transcripts above the black dashed lines exceed the library-specific 95th percentile ranking while those above the red line exceed the 99.9th percentile ranking.

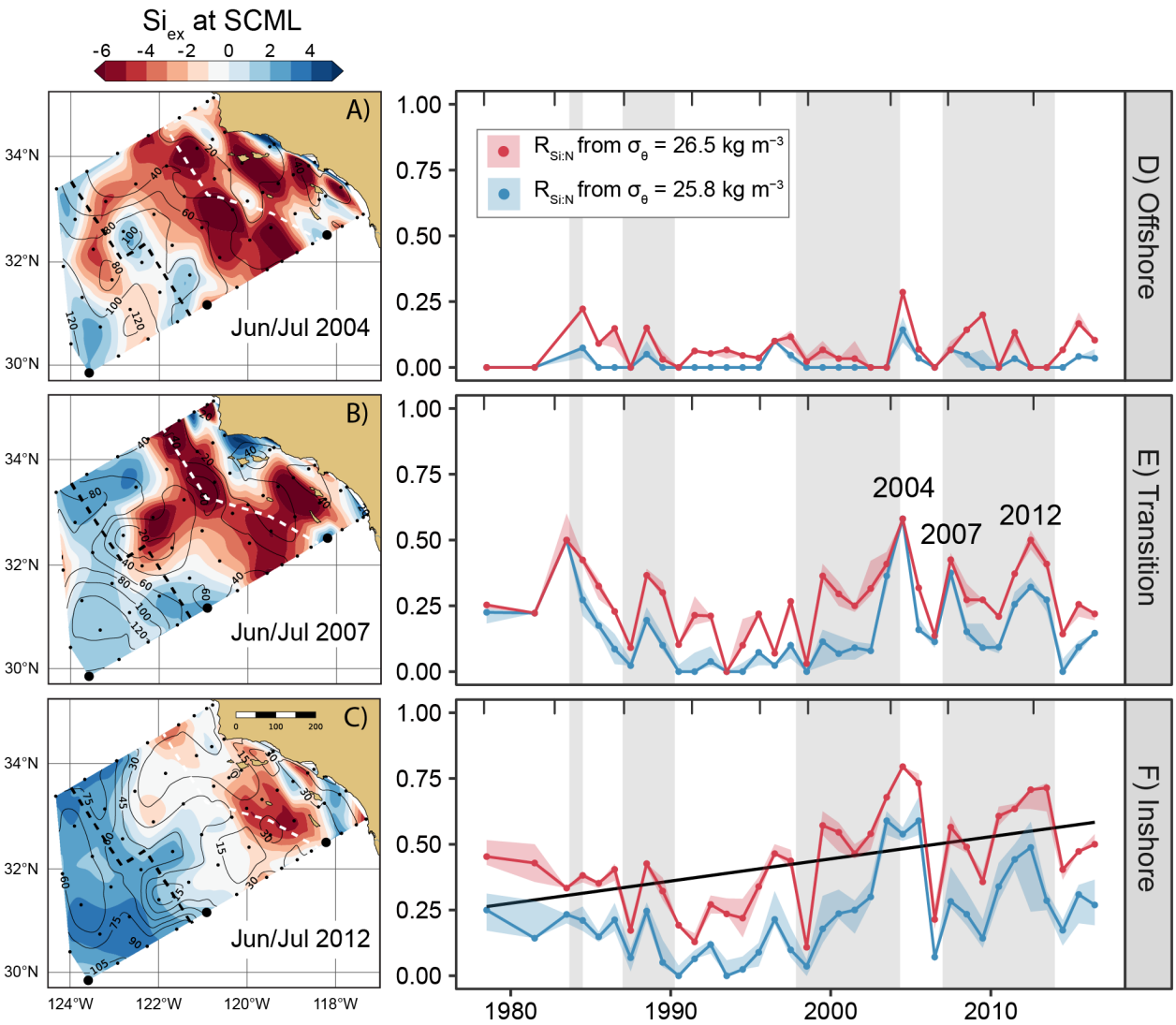

Fig. 4: Time series (1977-2017) of Si_{ex} at the SCML in the CalCOFI sampling area. Cubic-spline interpolated values of Si_{ex} at the depth of the SCML for A) Jun/July 2004 (season with most negative SCML Si_{ex} values), B) Jun/July 2007 (Approximate time of DCM07 cruise), and C) June/July 2012. Scale bar in C) represents 200 km. Black dots represent CalCOFI sampling stations used for the interpolation and large circles represent stations sampled for incubations and metatranscriptomes during the 2007 cruise. Black contour lines represent SCML depth and dashed lines represent Inshore-Offshore transitions. D-F) Spring-Summer (Apr-Sept) proportion of SCML samples with negative Si_{ex} values binned by geographic region. Colors represent Si_{ex} estimates based on the mean $R_{Si:N}$ ± S.D at two discrete upwelling isopycnals. Red: σ_θ = 26.5 kg m^{-3} and Blue: σ_θ = 25.8 kg m^{-3}. F) There is a significant monotonic increasing trend (nonparametric Mann-Kendall test P = 0.002) in the extent of negative Si_{ex} for the Inshore region (solid black line is linear regression). Shaded regions depict time periods where the three-year rolling mean of the NPGO is positive.

References:

1. Moore, J. K., Doney, S. C., Glover, D. M. & Fung, I. Y. Iron cycling and nutrient-limitation patterns in surface waters of the World Ocean. *Deep Sea Res. Part 2 Top. Stud. Oceanogr.* **49,** 463–507 (2001).
2. Tagliabue, A. *et al.* The integral role of iron in ocean biogeochemistry. *Nature* **543,** 51–59 (2017).
3. Hutchins, D. A. & Bruland, K. W. Iron-limited diatom growth and Si:N uptake ratios in a coastal upwelling regime. *Nature* **393,** 561–564 (1998).
4. King, A. L. & Barbeau, K. Evidence for phytoplankton iron limitation in the southern California Current System. *Mar. Ecol. Prog. Ser.* **342,** 91–103 (2007).
5. Brzezinski, M. A. *et al.* Enhanced silica ballasting from iron stress sustains carbon export in a frontal zone within the California Current. *J. Geophys. Res. C: Oceans* **120,** 4654–4669 (2015).
6. Browning, T. J. *et al.* Nutrient co-limitation at the boundary of an oceanic gyre. *Nature* (2017). doi:10.1038/nature24063
7. Raven, J. A. Predictions of Mn and Fe use efficiencies of phototrophic growth as a function of light availability for growth and of C assimilation pathway. *New Phytol.* **116,** 1–18 (1990).
8. Sunda, W. G. & Huntsman, S. A. Iron uptake and growth limitation in oceanic and coastal phytoplankton. *Mar. Chem.* **50,** 189–206 (1995).
9. Sunda, W. G. & Huntsman, S. A. Interrelated influence of iron, light and cell size on marine phytoplankton growth. *Nature* **390,** 389–392 (1997).
10. Strzepek, R. F. & Harrison, P. J. Photosynthetic architecture differs in coastal and oceanic diatoms. *Nature* **431,** 689–692 (2004).
11. Strzepek, R. F., Hunter, K. A., Frew, R. D., Harrison, P. J. & Boyd, P. W. Iron-light interactions differ in Southern Ocean phytoplankton. *Limnol. Oceanogr.* **57,** 1182–1200 (2012).

12. Nickelsen, L. & Oschlies, A. Enhanced sensitivity of oceanic CO2 uptake to dust deposition by iron-light colimitation. *Geophys. Res. Lett.* **42,** 2014GL062969 (2015).
13. Maldonado, M. T., Boyd, P. W., Harrison, P. J. & Price, N. M. Co-limitation of phytoplankton growth by light and Fe during winter in the NE subarctic Pacific Ocean. *Deep Sea Res. Part 2 Top. Stud. Oceanogr.* **46,** 2475–2485 (1999).
14. Boyd, P. W. *et al.* Control of phytoplankton growth by iron supply and irradiance in the subantarctic Southern Ocean: Experimental results from the SAZ Project. *J. Geophys. Res.* **106,** 31573–31583 (2001).
15. Boyle, E. A., Bergquist, B. A., Kayser, R. A. & Mahowald, N. Iron, manganese, and lead at Hawaii Ocean Time-series station ALOHA: Temporal variability and an intermediate water hydrothermal plume. *Geochim. Cosmochim. Acta* **69,** 933–952 (2005).
16. Sedwick, P. N. *et al.* Iron in the Sargasso Sea (Bermuda Atlantic Time-series Study region) during summer: Eolian imprint, spatiotemporal variability, and ecological implications. *Global Biogeochem. Cycles* **19,** GB4006 (2005).
17. Hopkinson, B. M. & Barbeau, K. A. Interactive influences of iron and light limitation on phytoplankton at subsurface chlorophyll maxima in the eastern North Pacific. *Limnol. Oceanogr.* **53,** 1303–1318 (2008).
18. Johnson, Z. I. *et al.* The effect of iron- and light-limitation on phytoplankton communities of deep chlorophyll maxima of the western Pacific Ocean. *J. Mar. Res.* **68,** 283–308 (2010).
19. Carr, M.-E. & Kearns, E. J. Production regimes in four Eastern Boundary Current systems. *Deep Sea Res. Part 2 Top. Stud. Oceanogr.* **50,** 3199–3221 (2003).
20. Stukel, M. R. *et al.* Mesoscale ocean fronts enhance carbon export due to gravitational sinking and subduction. *Proc. Natl. Acad. Sci. U. S. A.* (2017). doi:10.1073/pnas.1609435114
21. Aksnes, D. L. & Ohman, M. D. Multi-decadal shoaling of the euphotic zone in the southern sector of the California Current System. *Limnol. Oceanogr.* **54,** 1272–1281 (2009).

22. Kahru, M. & Mitchell, B. G. Influence of the 1997-98 El Niño on the surface chlorophyll in the California Current. *Geophys. Res. Lett.* **27,** 2937–2940 (2000).
23. King, A. L., Buck, K. N. & Barbeau, K. A. Quasi-Lagrangian drifter studies of iron speciation and cycling off Point Conception, California. *Mar. Chem.* **128–129,** 1–12 (2012).
24. Buck, K. N., Selph, K. E. & Barbeau, K. a. Iron-binding ligand production and copper speciation in an incubation experiment of Antarctic Peninsula shelf waters from the Bransfield Strait, Southern Ocean. *Mar. Chem.* **122,** 148–159 (2010).
25. Buck, K. N. & Bruland, K. W. The physicochemical speciation of dissolved iron in the Bering Sea, Alaska. *Limnol. Oceanogr.* **52,** 1800–1808 (2007).
26. Hogle, S. L., Bundy, R. M., Blanton, J. M., Allen, E. E. & Barbeau, K. A. Copiotrophic marine bacteria are associated with strong iron-binding ligand production during phytoplankton blooms. *Limnol Oceanogr Lett* **1,** 36–43 (2016).
27. Bruland, K. W., Rue, E. L. & Smith, G. J. Iron and macronutrients in California coastal upwelling regimes: Implications for diatom blooms. *Limnol. Oceanogr.* **46,** 1661–1674 (2001).
28. Sarmiento, J. L., Gruber, N., Brzezinski, M. A. & Dunne, J. P. High-latitude controls of thermocline nutrients and low latitude biological productivity. *Nature* **427,** 56–60 (2004).
29. King, A. L. & Barbeau, K. A. Dissolved iron and macronutrient distributions in the southern California Current System. *J. Geophys. Res.* **116,** C03018 (2011).
30. Sperfeld, E., Raubenheimer, D. & Wacker, A. Bridging factorial and gradient concepts of resource co-limitation: towards a general framework applied to consumers. *Ecol. Lett.* (2015). doi:10.1111/ele.12554
31. Dupont, C. L. *et al.* Genomes and gene expression across light and productivity gradients in eastern subtropical Pacific microbial communities. *ISME J.* **9,** 1076–1092 (2015).
32. McQuaid, J. B. *et al.* Carbonate-sensitive phytotransferrin controls high-affinity iron uptake in diatoms. *Nature* **555,** 534 (2018).

33. Allen, A. E. *et al.* Whole-cell response of the pennate diatom Phaeodactylum tricornutum to iron starvation. *Proc. Natl. Acad. Sci. U. S. A.* **105,** 10438–10443 (2008).
34. Morrissey, J. *et al.* A novel protein, ubiquitous in marine phytoplankton, concentrates iron at the cell surface and facilitates uptake. *Curr. Biol.* **25,** 364–371 (2015).
35. Chappell, P. D. *et al.* Genetic indicators of iron limitation in wild populations of Thalassiosira oceanica from the northeast Pacific Ocean. *ISME J.* **9,** 592–602 (2014).
36. Bertrand, E. M. *et al.* Phytoplankton–bacterial interactions mediate micronutrient colimitation at the coastal Antarctic sea ice edge. *Proceedings of the National Academy of Sciences* **112,** 9938–9943 (2015).
37. Cohen, N. R. *et al.* Diatom Transcriptional and Physiological Responses to Changes in Iron Bioavailability across Ocean Provinces. *Frontiers in Marine Science* **4,** 360 (2017).
38. Marchetti, A., Catlett, D., Hopkinson, B. M., Ellis, K. & Cassar, N. Marine diatom proteorhodopsins and their potential role in coping with low iron availability. *ISME J.* 1–4 (2015).
39. Landry, M. R. *et al.* Pelagic community responses to a deep-water front in the California Current Ecosystem: overview of the A-Front Study. *J. Plankton Res.* **34,** 739–748 (2012).
40. Rykaczewski, R. R. & Checkley, D. M., Jr. Influence of ocean winds on the pelagic ecosystem in upwelling regions. *Proc. Natl. Acad. Sci. U. S. A.* **105,** 1965–1970 (2008).
41. Lindegren, M., Checkley, D. M., Jr, Ohman, M. D., Koslow, J. A. & Goericke, R. Resilience and stability of a pelagic marine ecosystem. *Proc. Biol. Sci.* **283,** (2016).
42. Bograd, S. J. & Mantyla, A. W. On the subduction of upwelled waters in the California Current. *J. Mar. Res.* **63,** 863–885 (2005).
43. Gruber, N. *et al.* Eddy-induced reduction of biological production in eastern boundary upwelling systems. *Nat. Geosci.* **4,** 787–792 (2011).
44. Di Lorenzo, E. *et al.* North Pacific Gyre Oscillation links ocean climate and ecosystem change. *Geophys. Res. Lett.* **35,** (2008).

45. McGowan, J. A. *et al.* Predicting coastal algal blooms in southern California. *Ecology* **98,** 1419–1433 (2017).
46. Di Lorenzo, E. & Ohman, M. D. A double-integration hypothesis to explain ocean ecosystem response to climate forcing. *Proc. Natl. Acad. Sci. U. S. A.* **110,** 2496–2499 (2013).
47. Bakun, A. *et al.* Anticipated Effects of Climate Change on Coastal Upwelling Ecosystems. *Curr Clim Change Rep* **1,** 85–93 (2015).
48. Rykaczewski, R. R. & Dunne, J. P. Enhanced nutrient supply to the California Current Ecosystem with global warming and increased stratification in an earth system model. *Geophys. Res. Lett.* **37,** L21606 (2010).

Title: Pervasive iron limitation at subsurface chlorophyll maxima of the California Current

Authors: Shane L. Hogle[1]*, Christopher Dupont[2], Brian Hopkinson[3], Andrew L. King[4], Kristen N. Buck[5], Kelly L. Roe[6], Rhona K. Stuart[1,7], Andrew E. Allen[1,2], Elizabeth L. Mann[8], Zackary I. Johnson[9], Katherine A. Barbeau[1]

[1]Scripps Institution of Oceanography, La Jolla, California, USA

[2]J. Craig Venter Institute, La Jolla, California, USA

[3]Department of Marine Sciences, University of Georgia, Athens, GA, USA

[4]Norwegian Institute for Water Research, Bergen, Norway

[5]College of Marine Science, University of South Florida, St. Petersburg, FL, USA

[6]Finger Lakes Community College, Canandaigua NY, USA

[7]Lawrence Livermore National Laboratory, Livermore, CA, USA

[8]Bigelow Laboratory for Ocean Sciences, East Boothbay ME, USA

[9]Nicholas School of the Environment and Biology Department, Duke University Marine Laboratory, Beaufort, NC, USA

Corresponding author email: S.L.H (shogle@mit.edu) or K.A.B (kbarbeau@ucsd.edu)

*Present Address: Shane L. Hogle, Department of Civil and Environmental Engineering, Massachusetts Institute of Technology, Cambridge, Massachusetts, USA.

Supplementary Methods:

Sampling during the July 2007 cruise: We sampled all 15 CalCOFI stations along CalCOFI line 93.3 for hydrographic parameters (conductivity, temperature, pressure), oxygen concentrations, nitrate concentrations, silicic acid concentrations, and chlorophyll fluorescence with a CTD rosette. At stations 93.3/40, 93.3/80, and 93.3/120 we collected samples for total dissolved iron concentrations, iron-binding ligand concentrations, and incubation experiments using 30L trace-metal-clean GO-Flo bottles on non-metallic line[4,18,29]. We collected samples for community transcriptomes at three stations (93.3/40, 93.3/80, 93.3/120) at the depth of the SCML (30-110 m) using a CTD rosette. Details of the molecular sampling are described in a prior publication[31].

Incubation experiments from the July 2007 cruise: The seawater collection depth for the experiments was within the SCML near the start of the nitracline (initial concentrations of 2-10 μmol L^{-1} NO_3). We set up incubation experiments with triplicate or duplicate 4 L polycarbonate bottles, which we housed in a Percival incubator at 16°C with a 12:12 light:dark cycle. Our treatment scheme included two spectrally corrected light levels; an ambient light level (20 μE m^{-2} s^{-1}) and an elevated light level (80 μE $m^{-2}s^{-1}$). We set up triplicate bottles at ambient light conditions as unamended controls (Control) (Fig. 2, Supplementary Fig. 10) and as 2.5 nmol L^{-1} $FeCl_3$ additions (Fe). At elevated light levels we set up duplicate bottles as unamended controls (Light), 2.5 nmol L^{-1} Fe additions (Fe+Light), and 3.5 μmol L^{-1} Na_2SiO_3 (Si+Light, station 93.3/120 only). We sampled incubation bottles every 24 hours for chlorophyll, nutrients and Fv/Fm (Supplementary Fig. 10). We collected samples for primary production and phytoplankton (Supplementary Fig. 2) cell counts on the final day of the incubation experiments (9, 7, and 5 days for 93.3/120, 93.3/80, and 93.3/40, respectively). We preserved phytoplankton in formalin and counted the preserved cells onshore using phase contrast light microscopy. We measured primary production by radiolabeled ^{14}C incorporation on the final day of the incubation

53 experiments by incubating subsamples for 3 hours prior to measurement. The methods for
54 primary production estimates have been described in detail in an earlier publication and
55 references therein[31]. Photochemical conversion efficiency of PSII (Fv/Fm) was quantified using
56 single turnover fluorescence induction curves measured with a FIRe fluorometer (Satlantic) as
57 previously described[18].
58
59 **Biogeochemical measurements from the July 2007 cruise:** We measured silicate,
60 phosphate, nitrate, nitrite, and ammonium concentrations using an onshore autoanalyzer and
61 following the standard operating procedures from the California Current Ecosystem Long Term
62 Ecological Research (CCE-LTER) program (http://cce.lternet.edu/data/methods-manual). We
63 extracted chlorophyll *a* from GF/F filters using 90% acetone and subsequent incubation at -20°C
64 for 24 hours and then analyzed samples onboard the *R/V New Horizon* using a Turner Designs
65 Fluorometer. We measured dissolved iron concentrations using chemiluminescence flow-
66 injection analysis (FIA) with sulfite reduction[4,29], which has been demonstrated to be highly
67 sensitive and accurate with respect to SAFe and GEOTRACES consensus samples. We
68 measured the concentration and conditional binding strengths of organic iron-binding ligands
69 using standard established Competitive Ligand Exchange - Cathodic Stripping Voltammetry
70 (CLE-CSV) methods[25,49–51].
71
72 **Determining the NO_3:Fe ratio, nitracline, and ferricline depths from the July 2007 cruise:**
73 When NO_3:Fe values are greater than 8 µmol/nmol phytoplankton reliably respond to added Fe
74 by increasing nitrate consumption, cellular chlorophyll *a*, and total cell numbers[4,27]. Such
75 physiological shifts are diagnostic of Fe limited/stressed phytoplankton and are commonly
76 associated with diatom blooms after Fe fertilization in HNLC regions. We used NO_3:Fe values
77 greater than 8 µmol/nmol as a proxy for Fe limitation in our profiles (Fig. 1C). We also calculated

78 the depth of the nitracline and ferricline (Supplementary Table 1) from linearly interpolated
79 profiles using two different metrics: the depth of maximum rate of concentration change
80 (∂[nutrient]/∂z = max) and threshold concentrations of 1 μmol L^{-1} NO_3 and 0.2 nmol L^{-1} dissolved
81 iron[4,40]. In a few cases we misidentified the nutricline when using maximum ∂[nutrient]/∂z due to
82 steep gradients from densely sampled depth ranges with nutrient concentrations that were very
83 low or zero. We also found that ∂[nutrient]/∂z = max frequently placed the nitracline and
84 ferricline much deeper than we expected from the depth of the SCML and the associated
85 density profile. Since the SCML is frequently located at the shallowest depths of the nitracline
86 we decided to use threshold concentrations for defining the nitracline (1 μmol L^{-1} NO_3) and
87 ferricline (0.2 nmol L^{-1}) instead of using the maximum ∂[nutrient]/∂z approach, which we expect
88 would identify the 'core' of the nutracline from an ideal profile. These same threshold
89 concentrations have been commonly used in other studies of the southern California Current[4,40]
90 and represent what is commonly considered the 'top' of the nitracline and ferricline in this
91 region.
92
93 **Sequencing, quality control, and analysis of community transcriptomes from the July**
94 **2007 cruise:** The processes for collecting, storing, sequencing, quality control and annotation of
95 community DNA and RNA has already been described[31]. Briefly, we extracted total community
96 RNA (collected on a 0.2 μm filter and prefiltered at 20 μm) and utilized subtractive hybridization

of rRNAs[52] to generate rRNA-depleted total RNA. We then *in vitro* polyadenylated an aliquot of rRNA-depleted total RNA from stations 93.40, 93.80, and 93.120. We reverse transcribed this aliquot and a non-adenylated aliquot using oligo(dT) primers and sequenced the resulting cDNA from each aliquot using 454 pyrosequencing. We assembled reads from community transcriptomes *de novo* using CLC Genomics workbench and made gene calls on assembled contigs with FragGeneScan[53]. To determine transcript abundances, we filtered rRNA reads from the raw sequencing reads by searching reads against SILVA[54] and an in-house rRNA database using BLASTn (evalue 1e-5), and then removed artificial 454 sequencing duplicates using cd-hit-454[55]. We then recruited individual sequencing reads back to assembled contigs using best MegaBLAST[56] hits in order to obtain estimates of transcript abundance. To calculate library size and length normalized abundances we expressed transcript counts in Reads Per Kilobase of transcript per Million mapped reads (RPKM) units. We functionally annotated predicted genes from assembled transcripts using IMG[57], KEGG[57,58], Genbank[59], Ensembl[60], and the PyloDB database (https://github.com/allenlab/PhyloDB). To confirm the identity of the abundant pTF/ISIP3 transcripts we examined assembled contigs and aligned them to trusted pTF/ISIP3 sequences from marine eukaryotic genomes and transcriptomes [32]. In manually annotating pTF/ISIP3 sequences we made sure each contig was aligned to conserved amino acid residues in the full pTF or ISIP3 alignment [32]. We then taxonomically annotated all predicted genes using PhyloDB and the Automated Phylogenetic Inference System (APIS) as described before[61]. We excluded community genomes and transcriptomes from station 93.110 in order to focus on samples with paired incubation and trace metal data.

Acquisition and preprocessing of archival CalCOFI data: We downloaded data for the CalCOFI sampling grid (CalCOFI_Database_194903-201701) from the CalCOFI website (http://new.data.calcofi.org/index.php/reporteddata). The CalCOFI sample grid contains 113 stations from San Diego to San Francisco in the winter and spring (http://calcofi.org/field-

work/station-positions/113-station-pattern.html) and 75 stations from San Diego to north of Point Conception in the Summer and Fall (http://calcofi.org/field-work/station-positions/75-station-pattern.html). For each month and year we selected only samples from the 75 station grid (Fig. 1B) and then selected the months of April-September: the primary phytoplankton growing season. We excluded any samples that did not include chlorophyll, nitrate, and silicate measurements which resulted in 211,598 discrete bottle samples ranging from years 1978 to 2015. We then determined the depth of the SCML by finding the depth of the maximum chlorophyll *a* concentration for each sampling profile at each CalCOFI station. If multiple depths from the same profile had the same maximum chlorophyll *a* concentration we selected the deepest sampling bottle. This resulted in 11,161 discrete SCML bottle samples from the southern California Current.

Determining Si_{ex} from archival CalCOFI data and the July 2007 cruise: We determined the Si_{ex} tracer[5,20,29] at each depth of the SCML using a modified Si* formula[28,62]: Si_{ex} = [µmol silicate L^{-1}] - ([µmol nitrate L^{-1}] × $R_{Si:NO3}$). Si_{ex} modifies Si* by exchanging the original denitrification term for an estimated preformed molar silicic acid to nitrate ratio ($R_{Si:NO3}$) in coastal upwelled and wind stress curl upwelled source waters. We calculated Si_{ex} from $R_{Si:NO3}$ values determined at the σ_θ = 25.8 kg m^{-3} and σ_θ = 26.5 kg m^{-3} isopycnals, which represent the top and middle of the thermocline, respectively[63,64]. To account for temporal variability in $R_{Si:NO3}$ we determined the mean and standard deviation of $R_{Si:NO3}$ for all CalCOFI samples collected at σ_θ = 25.8 ± 0.1 kg m^{-3} and σ_θ = 26.5 ± 0.1 kg m^{-3} within five-year windows beginning at 1977. We then used these $R_{Si:NO3}$ mean and standard deviation values to determine Si_{ex} ± SD for each CalCOFI sample within each 5-year time frame.

Interpolation of biogeochemical parameters from CalCOFI data: We interpolated SCML depth, chlorophyll concentration, Si_{ex} at approximately 15 times the original sampling density

over the latitude range 30.18 to 15.09 °N and the longitude range 117.31 to 124.32 °W as converted to the Mercator projection (Fig. 4). Specifically, we interpolated values to a Mercator projected 1000 x 1000 grid using a twice continuously differentiable piecewise cubic polynomial function.

Derived Winds and Ocean Transports, Upwelling Index products, and the NPGO index: Values for the NPGO index[44] were downloaded from http://www.o3d.org/npgo/. Monthly upwelling, wind, and derived transport are from the Pacific Fisheries Environmental Laboratory (PFEL) and were downloaded from https://www.pfeg.noaa.gov/products/PFEL/modeled/indices/. The closest PFEL buoy location to the 75 station CalCOFI grid is at 33° N 119° W which most closely corresponds to Line 90.0 station 45 (32.918 ° N, 118.936° W) which is in the inshore sector of the CalCOFI grid. This location was used as a representative for the entire CalCOFI 75 station grid.

Statistical Tests: To determine significant distributional changes within transport, wind, and upwelling time series we used Nonparametric Multiple Change Point Analysis implemented in the R package ecp[65]. This allowed us to identify times where one of these parameters had shifted significantly relative to past observations. To determine correlations between biogeochemical parameters and climatological/physical parameters we calculated the cross-correlation of paired univariate time series as well as Pearson's rank correlation. All time series were scaled to a mean of zero and standard deviation of one, then differenced by a time lag of one month to remove temporal autocorrelations (as assessed through an Augmented Dickey–Fuller test as well as the Kwiatkowski-Phillips-Schmidt-Shin (KPSS) test). To test for monotonically increasing trends in time series we used the nonparametric Mann-Kendall test.

Supplementary results and discussion:

Study region: The 700 km transect from July 2007 (Fig. 1B) followed the southernmost line (Line 93.3) of the California Cooperative Oceanic Fisheries Investigations (CalCOFI, calcofi.ucsd.edu) sampling grid. We sampled 15 oceanographic stations in the southern California Current (CC), which featured a strong productivity gradient from the highly productive waters on the narrow continental shelf, to mesotrophic water at the edge of the continental shelf, and finally to oligotrophic water in the eastern subtropical Pacific Ocean[66]. Here we refer to these stations within the context of a geographic classification scheme typical for the region (see main text and Fig. 1B)[21,22,66]. At the Inshore CC sector (Fig. 1B) coastal alongshore winds drive intense springtime Ekman upwelling[67] leading to high ecosystem productivity and net carbon export[40]. The size spectrum of plankton at the Inshore sector is dominated by larger bodied diatoms and mesozooplankton, especially at the onset of spring upwelling and the injection of new nutrients. Typically, in the CC diatoms decrease in abundance as the summer progresses and nutrient pulses from springtime upwelling are consumed. The southern CC Transition zone begins approximately 100-200 km offshore where Ekman upwelling subsides and cyclonic wind-stress curl upwelling becomes more prominent resulting in a reduced plankton size spectrum. In the Offshore zone of the Southern CC wind-stress and Ekman upwelling are greatly attenuated and conditions are similar to those in the oligotrophic North Pacific gyre where small phytoplankton such as picoeukaryotes and picocyanobacteria dominate.

Definitions of limitation, co-limitation, and stress: In this study we present a variety of evidence derived from transcriptomes, biogeochemical proxies, and trace-metal-clean nutrient amendment bioassay experiments for the effects of Fe and Fe/light on phytoplankton communities in the southern CC. The gold standard for diagnosing the trace metal nutritional status of marine phytoplankton communities is via direct experimental nutrient amendments using trace metal-clean seawater incubations, which we conducted for three discrete SCML

samples on CalCOFI line 93.3. In these experiments the terminology of 'limitation' or 'co-limitation' is applicable as they were conducted within a testable experimental treatment/control framework. In contrast our transcriptomes and biogeochemical proxies were assessed *in situ* outside of an experimental/control framework and in the case of Si_{ex}, over a 40-year time series. Here we define stress and limitation after Moore *et. al*[68]. Specifically stress is an observed physiological consequence of nutrient scarcity (for example high concentrations of Fe-stress transcripts or water column Si deficiencies relative to NO_3), while limitation is an observed restriction of the growth rate for individual cells and/or the carrying capacity of a system because of the deficiency of one or more nutrients. In the context of this study we use the terms 'limitation' and 'co-limitation' when referring to the results from our factorial nutrient-amended incubations and the term 'stress' to encompass a broader multitude of Fe effects inferable from biogeochemical proxies and biological sequence data. As the concepts of both 'stress' and 'limitation' exist along the same resource utilization continuum, this then allows us to discuss the results from this study in an contextualized and integrative but conceptually-precise framework.

We observed evidence for multiple nutrient limitation and co-limitation scenarios in our incubation experiments, and we present here brief definitions of co-limitation as relevant to our study. This nomenclature is largely consistent with that proposed in prior studies of ecological systems[6,30,68,69].

Single limitation: Growth is limited by a single non-substitutable resource (Resource A) that has been drawn down to levels where addition of only this resource produces a growth response. No other resources (Resources B or C) added in combination with Resource A produce a positive growth response greater than that of Resource A. An example of single limitation is Fe-limitation in HNLC regions where macronutrients accumulate in surface waters and only the

addition of Fe can stimulate growth and macronutrient drawdown[70]. We likely did not observe this type of limitation response in our incubations.

Serial limitation: Also known as secondary limitation. Only addition of Resource A produces a positive response, but addition of Resource B in combination with Resource A produces a larger response than Resource A alone. Serial limitation may emerge when phytoplankton growth, and light harvesting is limited by the availability of Fe. Here Fe is the proximally limiting nutrient, but light quickly becomes limiting after Fe becomes replete. Phytoplankton communities from incubations at station 93.3/40 were serially limited by Fe and then light. Fe+Light increased total chlorophyll to the greatest extent, the addition of Fe alone stimulated a more moderate increase and solely increasing light had no significant effect. Fe+Light and Fe alone both stimulated a similar increase in photosynthetic efficiency. Fe+Light stimulated the greatest nitrate drawdown while the addition of Fe to Inshore water stimulated nutrient drawdown to a much greater extent than light alone. Changes in primary production mirrored the nitrate consumption trend thus strongly indicating serial Fe, light limitation in the Inshore zone.

Independent co-limitation: The addition of both Resource A and Resource B individually produces a positive growth response, and the addition of A+B together produces a larger growth response than A or B individually. Independent co-limitation may emerge when phytoplankton light harvesting is limited by the availability of Fe and phytoplankton growth is limited by the availability of light. Additional light or Fe can partially compensate for the lack of the complementary resource, but photosynthetically replete conditions only develop with an increase in both resources simultaneously[17]. Independent co-limitation by Fe/light may manifest through physiological trade-offs between demand, allocation efficiency, and/or uptake mechanisms of these two resources[30,71]. Phytoplankton communities from incubations at station 93.3/80 were independently co-limited by Fe and light where the greatest growth stimulation

252 came from added Fe+Light. Total chlorophyll and photosynthetic efficiency responses of
253 phytoplankton were similar to the patterns seen at the Inshore zone. In both cases, Fe+light
254 increased total chlorophyll to the greatest extent, the addition of Fe alone stimulated a more
255 moderate increase and solely increasing light had no significant effect. In contrast, responses
256 between the two study-sites were different for nitrate drawdown and PP. Fe+light stimulated the
257 greatest nitrate drawdown in both stations 93.3/40 and 93.3/80, However, nitrate consumption in
258 the outer transition zone increased modestly and to the same extent when either Fe or light was
259 added alone, while the addition of Fe to Inshore water stimulated nutrient drawdown to a much
260 greater extent than light alone. Changes in primary production mirrored the nitrate consumption
261 trend. The similar responses to both iron and light added individually at the Transition zone
262 (93.3/80) are most consistent with an independent co-limitation scenario.
263
264 *Simultaneous co-limitation:* Also known as 'true' co-limitation. This occurs when both Fe and
265 light are so scarce that growth is impossible without a supply of both resources
266 simultaneously[72]. The incubation results from the Offshore zone
267 at 93.3/120 likely represent simultaneous co-limitation since Fe+light had the largest effect,
268 while neither resource alone produced significant change from the control.
269
270 **Si_{ex} as a biogeochemical proxy for diatom Fe limitation:** The Si_{ex} proxy traces shifts in the
271 ratio of $Si(OH)_4$ to NO_3 in the euphotic zone due to the preferential uptake of $Si(OH)_4$ by Fe-
272 limited diatoms. Diatoms acquire nitrate and silicic acid at roughly an equimolar ratio when
273 grown in nutrient replete conditions[73], but under Fe limitation they are well known to utilize
274 excess silicic acid relative to nitrate[3,74,75]. In the euphotic water column deviations of the $Si:NO_3$
275 ratio from a preformed upwelling value should thus reflect biological uptake in the euphotic zone
276 assuming nitrification and denitrification in the euphotic zone is negligible[28]. Positive Si_{ex} values
277 imply that non-silicifying phytoplankton consume the bulk of nitrate, while negative Si_{ex} values

imply dominant diatom growth under Fe stress/limitation. Zero Si_{ex} values reflect replete diatom growth or may also reflect a balance of nutrient supply and biological removal by Fe-limited diatoms and non-silicifying phytoplankton averaged over the phytoplankton community. However, Si_{ex} can only be interpreted as an index of diatom growth under Fe-limitation and not as a community-wide Fe-limitation index, though diatoms dominate the responses to Fe+light here and elsewhere[18].

Selecting appropriate density horizons for upwelled source waters: Si_{ex} depends on the preformed ratio ($R_{Si:NO3}$) of Si and NO_3 from upwelled source waters (supplementary methods). To calculate Siex at each station we empirically determined $R_{Si:NO3}$ from two upwelling density surfaces representing the top (σ_θ = 25.8 kg m^{-3}) and center (σ_θ = 26.5 kg m^{-3}) of the thermocline. The σ_θ = 26.5 kg m^{-3} surface generally penetrates deeper into water column than σ_θ = 25.8 kg m^{-3}. Both density surfaces can shoal well into the upper euphotic zone during upwelling season and have $R_{Si:NO3}$ values roughly at unity below 100 meters depth (Supplementary Fig. 11). In the CalCOFI sampling region the σ_θ = 25.8 kg m^{-3} isopycnal surface is typically located at the top of the thermocline whereas the σ_θ = 26.5 kg m^{-3} isopycnal surface represents a central-thermocline salinity maximum associated with the California Undercurrent[63,76,77]. The σ_θ = 26.5 kg m^{-3} isopycnal ventilates in the western subarctic Pacific and does not outcrop in the California Current during winter[64], which generally isolates it from mixed-layer biogeochemical processes. Results presented in the main and supplementary figures are derived from $R_{Si:NO3}$ at the σ_θ = 26.5 kg m^{-3} isopycnal surface, but all analyses were also performed using $R_{Si:NO3}$ determined at σ_θ = 25.8 kg m^{-3}, which represents an $R_{Si:NO3}$ minimum. Si and NO_3 were in approximately equal proportions at σ_θ = 25.8 kg m^{-3} (temporally and spatially averaged $R_{Si:NO3}$ = 0.99 ± 0.08), whereas Si often exceeded NO_3 at σ_θ = 26.5 kg m^{-3} (temporally and spatially averaged $R_{Si:NO3}$ = 1.30 ± 0.05). Temporal and spatial trends were largely insensitive to different $R_{Si:NO3}$ values (Fig. 4D-F), but $R_{Si:NO3}$ from σ_θ = 26.5 kg m^{-3} resulted in more negative Si_{ex} values at the SCML.

Regardless, modifying $R_{Si:NO3}$ within the range of σ_θ = 25.8-26.5 kg m^{-3} resulted in no change of the general trends displayed Fig. 4 and Supplementary Figs. 5,7, and 9.

The specificity of the Si_{ex} proxy for diatom Fe-limitation: Although the Si_{ex} proxy is potentially sensitive to processes other than diatom Fe-limitation, we argue that it is a robust indicator for Fe-limitation within the scope of this study and largely resistant to the effects of mixing, shifts from coastal Ekman upwelling to wind stress curl upwelling, and potential nitrification at the SCML. We address each of these points below.

Temporal variability: There is evidence that the source waters upwelled into the CalCOFI sampling grid have changed over the last 40 years[63] which could potentially have an effect on $R_{Si:NO3}$ used to calculate Si_{ex}. Indeed, our results show that $R_{Si:NO3}$ has shifted somewhat at densities typical for upwelled source waters, particularly at the 25.8 σ_θ kg m^{-3} isopycnal (Supplementary Fig. 12). For example, the mean $R_{Si:NO3}$ at 25.8 σ_θ kg m^{-3} during 1992-1997 is higher than that for 2002-2007. To account for temporal variability in $R_{Si:NO3}$ we determined the mean and standard deviation of $R_{Si:NO3}$ for all CalCOFI samples collected at σ_θ = 25.8 ± 0.1 kg m^{-3} and σ_θ = 26.5 ± 0.1 kg m^{-3} within five-year windows beginning at 1977. We then used these $R_{Si:NO3}$ mean and standard deviation values to determine Si_{ex} ± SD for each CalCOFI sample within each 5-year time frame. Si_{ex} values from the entire CalCOFI data set had effectively no correlation with the $R_{Si:NO3}$ ratio at either σ_θ = 25.8 kg m^{-3} or σ_θ = 26.5 kg m^{-3} (Supplementary Fig. 9). Furthermore, even assuming upwelled waters are sourced from the top of the thermocline (σ_θ = 25.8 kg m^{-3}), the patterns of increasingly negative SCML Si_{ex} values during the 2000s are robust (Fig. 4F). We believe that performed $Si:NO_3$ ratios determined from the middle of the thermocline (σ_θ = 26.5 kg m^{-3}) are more appropriate given that this density surface does not outcrop in the California Current during winter isolating it from the effects of mixed-layer biological processes[64]. Regardless, the observed patterns at either density horizon support our

contention that negative Si_{ex} values at the SCML are the result of *in situ* Si and NO_3 consumption rather than variation in the composition of upwelled source waters over time.

Effects of mixing and lateral advection: Although mixing between upper ocean water masses carrying negative Si_{ex} signals from elsewhere could, in theory, obscure *in situ* biological processes, there is no evidence that the negative Si_{ex} signals observed in our study are the result of diapycnal or isopycnal water mass mixing. Offshore waters had highly depleted nitrate and horizontal mixing between inshore and offshore would have served to increase Si_{ex} values. In the upper 50 meters of the inshore and transition zones there was usually an excess of silicate relative to nitrate, and the negative Si_{ex} signal was only evident at depths surrounding the SCML (Fig 1, Supplementary Fig. 7). Furthermore, waters of the main thermocline in the Pacific Ocean (the North Pacific Intermediate water) are sourced from high nutrient water in the ocean interior where the Si concentrations exceed those of NO_3; sometimes by up to a factor of 20 or more[28]. Therefore, upwelled water from the main thermocline in CC region should have excess Si relative to NO_3, and vertical mixing should serve to counteract processes generating a negative Si_{ex} signal. There was no significant correlation between $R_{Si:NO3}$ ratio and salinity/density in the upper 250 meters of the water column (Supplementary Figs. 9,11) confirming that negative Si_{ex} values are not dependent upon water mass tracers in the CC euphotic zone. Furthermore, the tight localization of negative Si_{ex} values to the depth range of the SCML and the base of the euphotic zone in the inshore and transition zones provides compelling evidence that the signal is derived from biological processes endemic to the SCML. Another consideration is whether Si_{ex} signals reflect local or remote diatom Fe-limitation. Subduction and transport of formerly diatom Fe-limited waters from northern upwelling regions could potentially imprint negative Si_{ex} signals on southern SCMLs, but the negative Si_{ex} signal would then still come from diatom Fe-limitation and not a different biogeochemical process. Backtracking the exact location of diatom Fe-limitation is outside the scope of this study, but

356 newer methods that infer spatially resolved rates of tracer change from submesoscale and
357 mesoscale circulation patterns may be appropriate[78].
358
359 *Effects of upwelling intensity and nutrient remineralization time/length scales:* A significant
360 fraction of the nutrient supply to the Transition and Offshore zones is from wind stress curl
361 upwelling rather than coastal upwelling, particularly later in the season as strong along shore
362 winds weaken along with the associated coastal Ekman upwelling. Wind stress curl upwelling
363 delivers weak but sustained pulses of water from more shallow sources compared with coastal
364 Ekman upwelling. Due to differences in remineralization length scales for macro and
365 micronutrients[79] these shallow source waters may have different *in situ* $R_{Si:NO3}$ than deeper
366 waters from the σ_θ = 25.8 kg m^{-3} or σ_θ = 26.5 kg m^{-3} surfaces. For example, nitrogen is generally
367 recycled to nitrate faster than silicate from sinking diatoms thus potentially decreasing $R_{Si:NO3}$ at
368 the more shallow wind-stress curl upwelling horizons.
369
370 Although nitrification has conventionally been assumed to be confined to the dark ocean, recent
371 work has demonstrated the occurrence of nitrification within the euphotic zone[80–83]. In the
372 northern CC the highest nitrification rates are often observed just below the euphotic zone[82,83]
373 and have been measured at maximal rates from approximately 0.1-0.2 mmol m^{-3} day^{-1}. If a
374 significant amount of nitrification occurs above the σ_θ = 25.8 kg m^{-3} or σ_θ = 26.5 kg m^{-3}
375 isopycnals (in the euphotic zone or just below it) and if the rate of biogenic nitrogen and silicate
376 recycling is strongly decoupled[79] Si_{ex} could be artificially pushed in the negative direction simply
377 due to internal recycling and circulation effects. However, upwelling rates are relatively high in
378 the CC (particularly in the Inshore and nearshore Transition zones), and nitrate supply to the
379 euphotic zone is likely to be dominated by new nitrate supplied from below the euphotic zone.
380 Indeed, *in situ* nitrification in the euphotic zone and just below it would be approximately 0.7% of

the upwelled nitrate supply assuming a mean upwelled supply rate of 10 mmol m^{-3} day^{-1} which is reasonable for much of the CC region[84,85].

We acknowledge that some component of the pervasive negative Si_{ex} signature identified in this study likely comes from nitrification in the euphotic zone and decoupled Si remineralization, but we stress that the majority of the signal must derive from *in situ* diatom Fe limitation. Shifts in the dominant mode of upwelling from coastal Ekman to curl-driven could potentially change the density horizon from which upwelled water is sourced from those used in our study (σ_θ = 25.8 kg m^{-3} or σ_θ = 26.5 kg m^{-3} isopycnals). We did not attempt to correct for curl vs. coastal upwelling since it is difficult to decipher the dominant upwelling mode from CalCOFI bottle samples and casts. However, we note that varying the value of $R_{Si:NO3}$ to as low as 0.8 (20% more NO_3 than Si in source waters) in our initial sensitivity tests still resulted in approximately the same number of Inshore and Transition zone SCML samples with negative Si_{ex} values, which generally suggests that when Si_{ex} is negative NO_3 greatly exceeds $Si(OH)_4$ concentrations. Furthermore, the outer transition zone and Offshore zone are regions where curl upwelling dominates nutrient supply rarely, but they rarely displayed negative Si_{ex} values in the CalCOFI time series (Supplementary Figs. 4,5). This suggests that correcting $R_{Si:NO3}$ downward in an attempt to compensate for shallow curl upwelling horizons would not impact our results and general conclusions in these regions.

Materials & Data Availability: All data supporting the findings of this study are available the following websites. CalCOFI time series data are available from the CalCOFI data archives (http://new.data.calcofi.org/index.php/reporteddata). Metatranscriptome and metagenome biological sequence files are available from iMicrobe (https://imicrobe.us, iMicrobe project ID: CAM_P_0001069). Biogeochemical data subsets, metatranscriptome annotations, and all computer code required to reproduce the results reported in this study are available from

Figshare (https://doi.org/10.6084/m9.figshare.6033761.v1) and Github (https://github.com/slhogle/DCM2007). Complete and unprocessed biogeochemical data are available from the UCSD Datazoo Research Project (http://oceaninformatics.ucsd.edu/datazoo/catalogs/ccelter/sources/1758).

Supplementary Table 1: Nutricline Depths

Station	Depth maximum $\partial[NO_3]/\partial z$	Depth maximum $\partial[dFe]/\partial z$	Depth where $[NO_3]$ = 1 μmol L^{-1}	Depth where [dFe] = 0.2 nmol L^{-1}
93.3/40	35 m	85 m	31 m	74.3 m
93.3/80	125 m	72.5 m	66 m	78.6 m
93.3/120	170 m	195 m	120 m	194 m

Depths of the ferricline and nitracline at each incubation and metatranscriptome sampling station as defined by two different metrics: depth of maximum rate of concentration change (∂[nutrient]/∂z = max) and and threshold concentrations (1 μmol L^{-1} NO_3 and 0.2 nmol L^{-1} dFe).

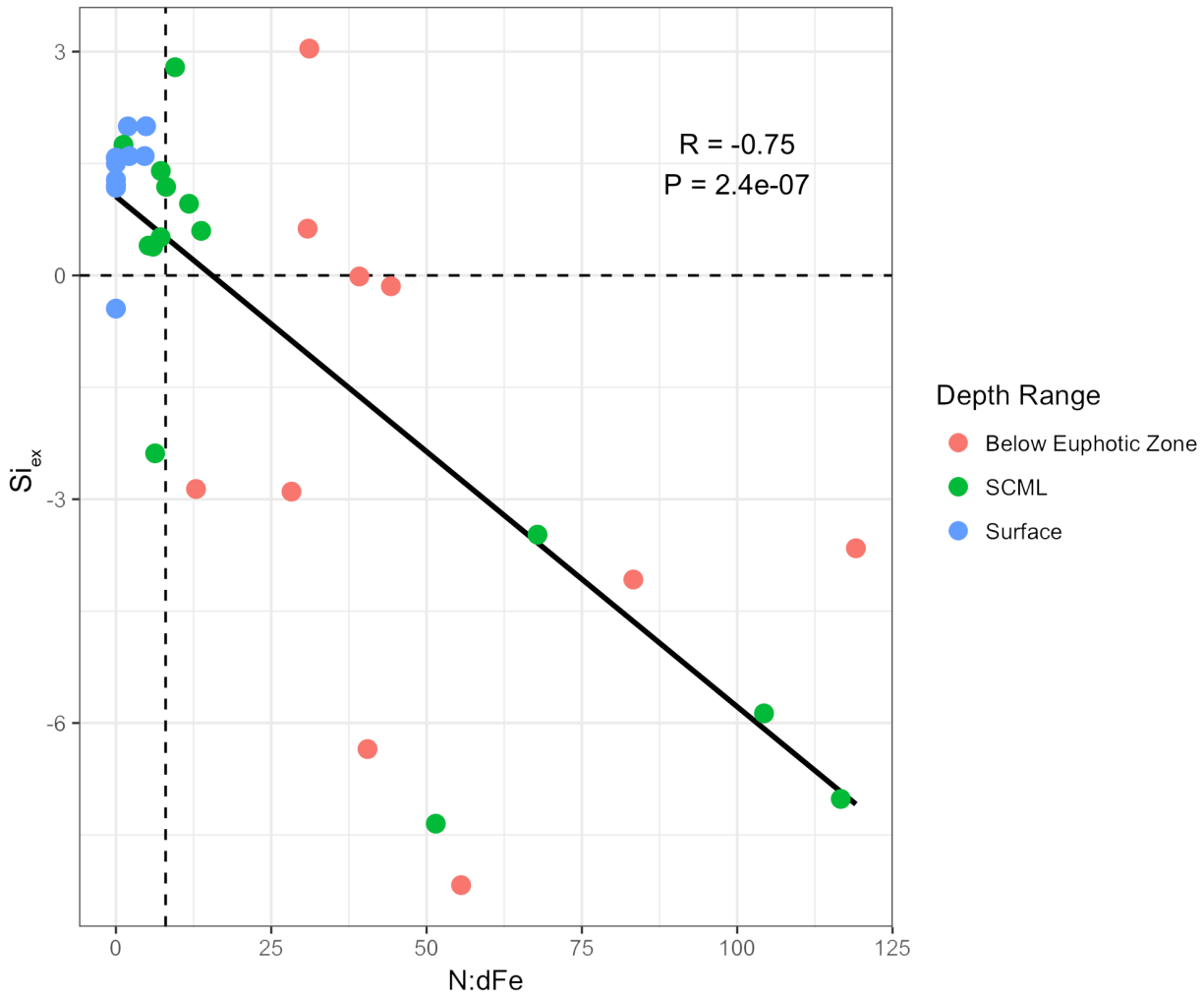

Supplementary Fig. 1: Relationship between Si_{ex} and the NO_3:dFe ratio from all samples taken during the July 2007 cruise. Point color depicts sample depth range (Surface, samples shallower than SCML; SCML, samples ± 10 meters of SCML depth; Below Euphotic Zone, samples from depths with light irradiance < 1% of surface values). Dashed lines represent diatom Fe-limitation thresholds (Si_{ex} < 0; N:dFe > 8). Pearson's product-moment correlation and associated *P* value are displayed in the upper right corner.

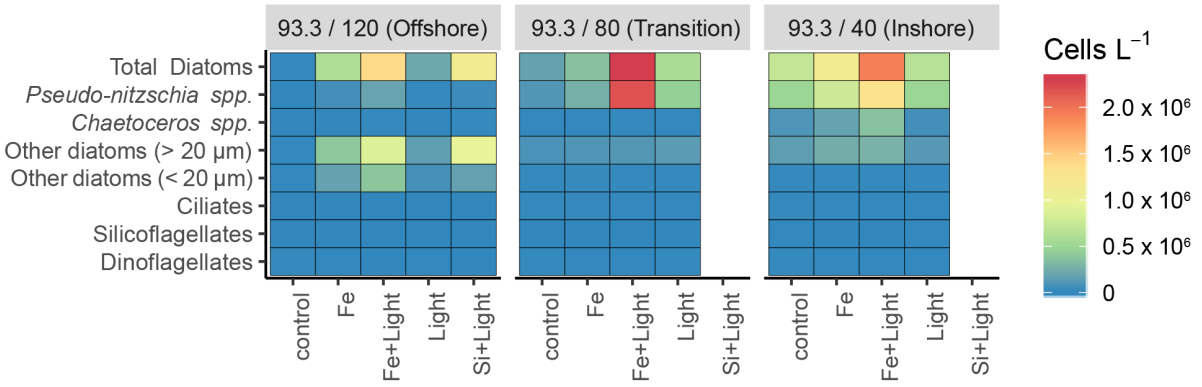

Supplementary Fig. 2: Abundances of phytoplankton groups as determined by microscopy from each incubation. The horizontal axis represents different incubation conditions (Si treatments were not performed at Transition and Inshore stations.The vertical axis represents the eight most abundant phytoplankton groups detected in the incubations. Color represents cell concentration (cells L^{-1}). Si+Light treatments were only included at station 93.3/120. Each cell represents the mean of biological triplicates or duplicates.

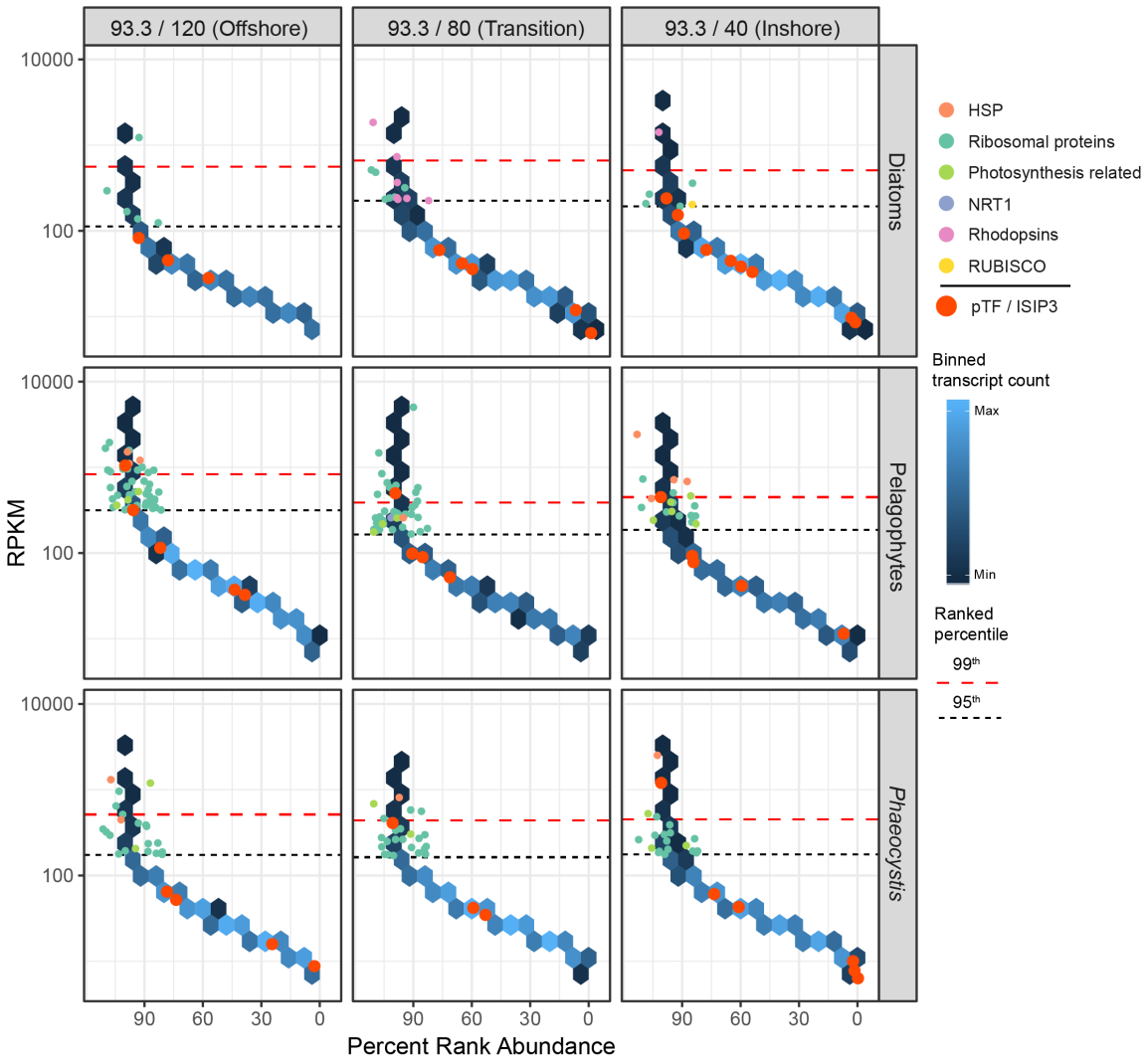

Supplementary Fig. 3: Rank abundance plots for total assembled transcripts from three taxonomic groups (Diatoms, Pelagophytes, and Phaeocystis) of each SCML metatranscriptome sample. Position on the vertical axis (log10 scale) depicts the reads per kilobase of transcript per million mapped reads (RPKM) and horizontal axis equals the windowed percentile transcript ranking per taxonomically resolved metatranscriptome. Each hexagonal bin depicts a spatial histogram on the RPKM vs Rank abundance grid and the color of each bin is proportional to the number of binned transcripts count within that gridded area. Individual pTF/ISIP3 transcripts at or above the 95th percentile ranking for each metatranscriptome are denoted by red points. For additional context, other colored points represent transcripts associated with a selection of essential cellular processes (HSP, Heat Shock Proteins; Ribosomal proteins, all detected ribosomal assembly protein subunits; Photosynthesis related, Photosystem reaction center proteins (*psbE,F,H-N,R,S,W*), light harvesting complex proteins (chlorophyll a/b/c or fucoxanthin binding); RUBISCO, Ribulose-1,5-bisphosphate carboxylase) and other biogeochemically relevant processes (NRT1, nitrate transporter; Rhodopsins, Eukaryotic rhodopsin-like genes). Transcripts above the black dashed lines exceed the taxonomy/library-specific 95th percentile ranking while those above the red line exceed the 99.9th percentile ranking.

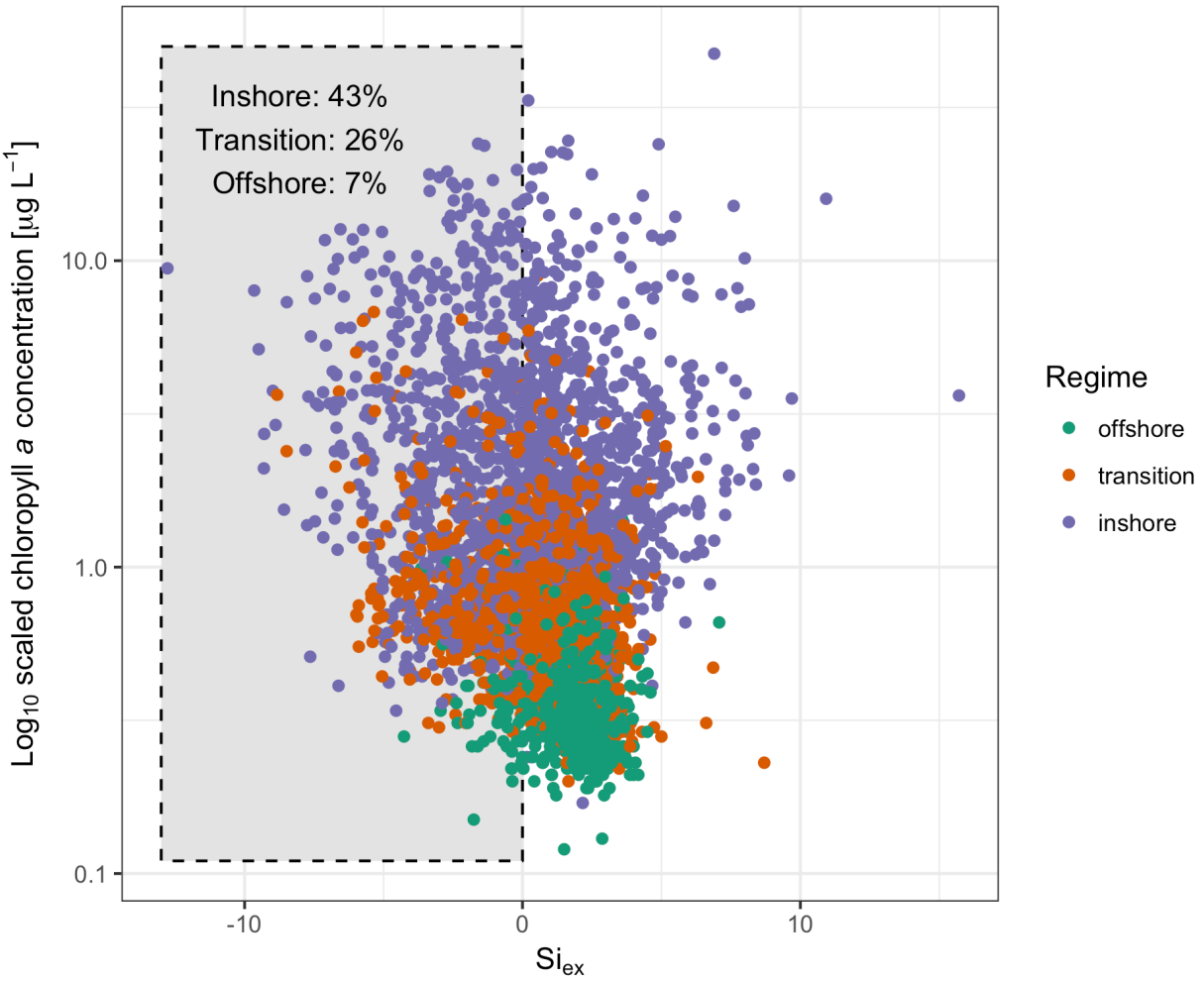

Supplementary Fig. 4: 40 years of SCML Si_{ex} values plotted against chlorophyll *a* concentrations (log_{10} scaled). Each sample is colored by its geographic/oceanographic regime. The shaded region encloses all samples with negative Si_{ex} values, and the proportion of SCML samples with negative Si_{ex} values in each geographic regime displayed in the upper left corner.

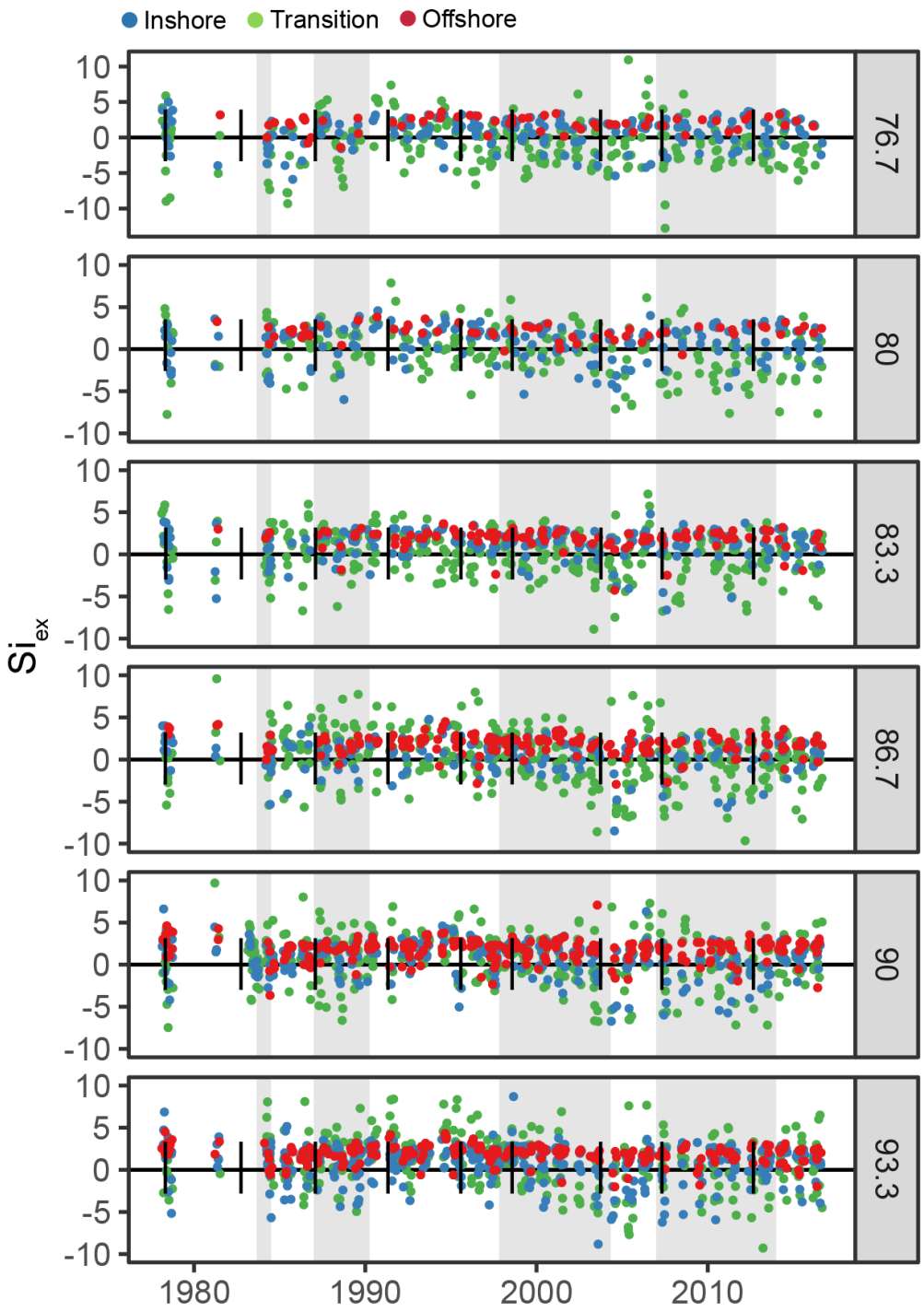

Supplementary Fig. 5: Si_{ex} at the SCML depth from 1978 to 2017 at each CalCOFI station binned by line arranged north to south. Each SCML sample is colored according to geographical region (Inshore = blue, Transition = green, Offshore = red). Shaded regions highlight durations when the NPGO rolling mean is positive (see Supplementary Fig. 8). Vertical black lines indicate times where Nonparametric Multiple Change Point Analysis [65] indicated a significant distributional change of the NPGO rolling mean. Change point analysis roughly partitions the periods of positive and negative NPGO index values.

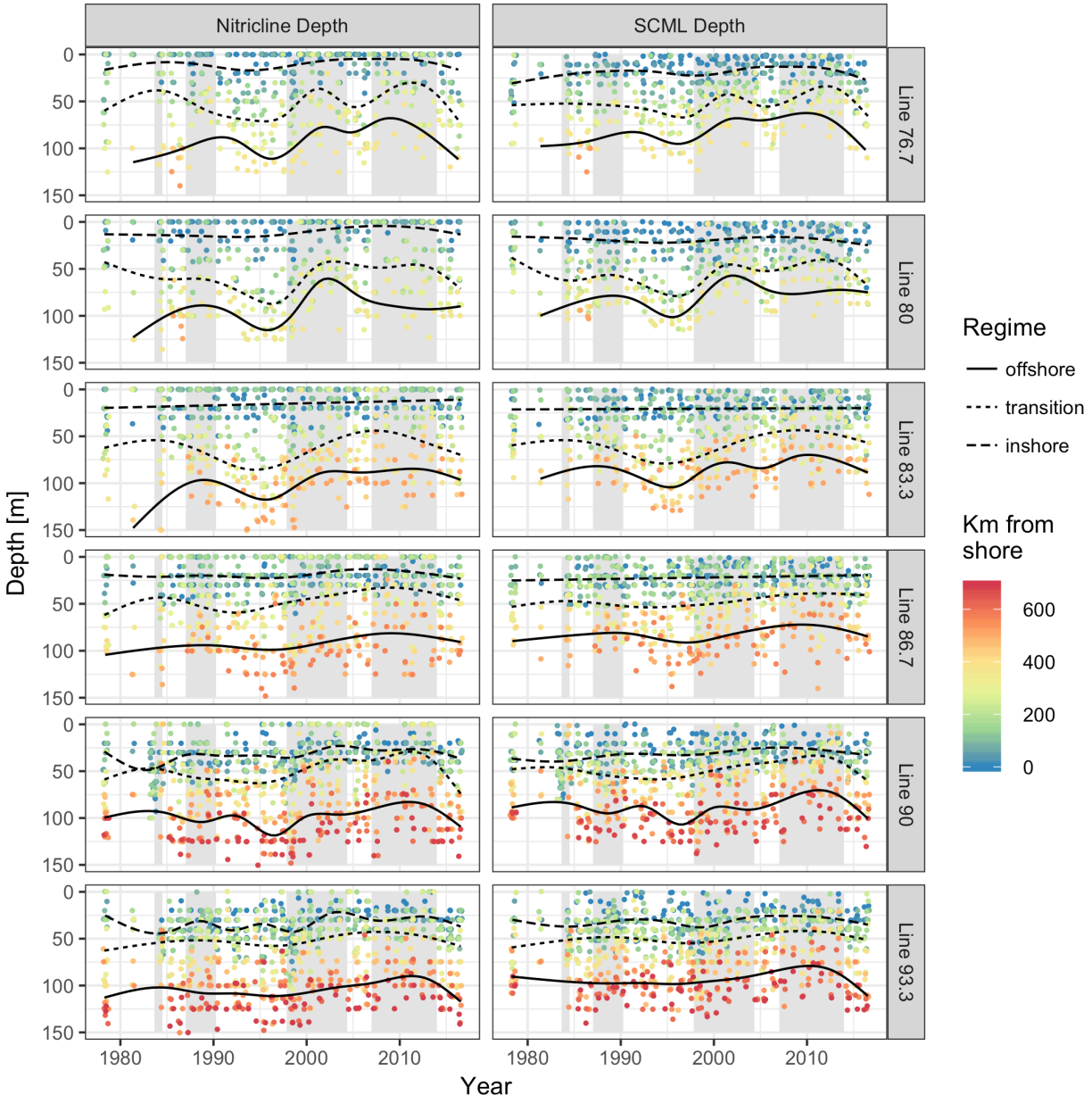

Supplementary Fig. 6: Nitracline Depth (determined using a threshold concentration of 1 μmol L^{-1} NO_3) and SCML Depth from 1978 to 2017 facetted by CalCOFI line (lines arranged north to south). Each discrete sample is colored according to the linear distance (km) from shore along its parent line. Lines are smoothed fits for all samples within the Inshore-Offshore geographic classification scheme in Fig. 1B. Smooths are derived from generalized additive models using cubic regression splines with 10 degrees of freedom. Shaded regions highlight durations when the NPGO rolling mean is positive (see Supplementary Fig. 8).

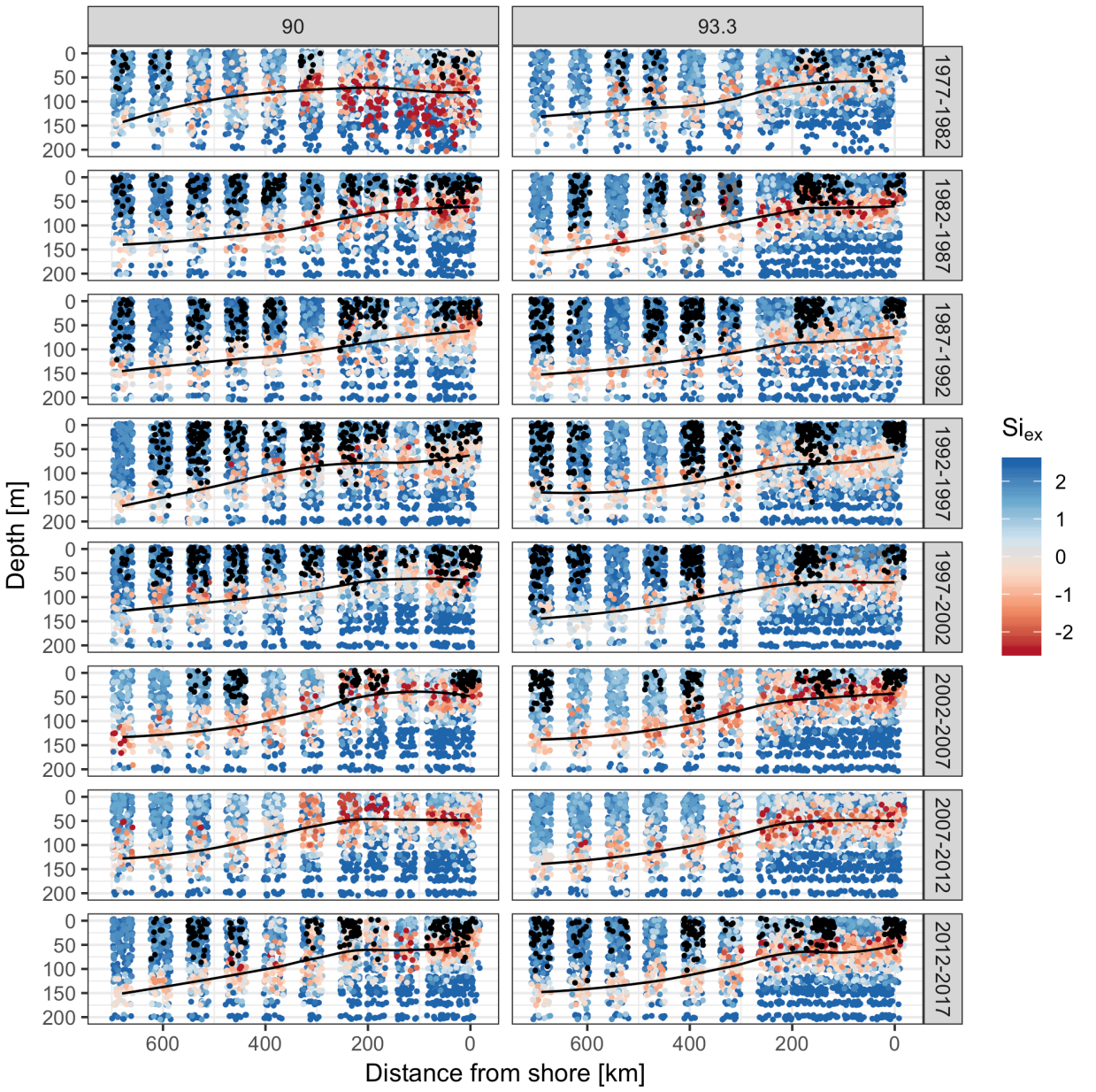

Supplementary Fig. 7: Si_{ex} values for CalCOFI lines 90.0 and 93.3 binned by five-year windows beginning in 1977. Vertical axis is depth (meters) and horizontal axis is linear distance (km) from shore along each CalCOFI line. Si_{ex} values are calculated using the $R_{Si:NO3}$ ratio from the σ_θ = 25.8 kg m^{-3} potential density horizon. Si_{ex} calculated at σ_θ = 26.5 kg m^{-3} displays the same pattern as shown here but with a greater magnitude of negative values over a greater depth range. CalCOFI samples with available light measurements (~8% of samples) and with light intensities greater than 1% of incident irradiance are overlaid as black points to highlight the approximate extent of the euphotic zone. Solid lines track the center of the negative Si_{ex} "band" at each CalCOFI line and are smoothed fits derived from generalized additive models of negative Si_{ex} sample depths using cubic regression splines with 10 degrees of freedom.

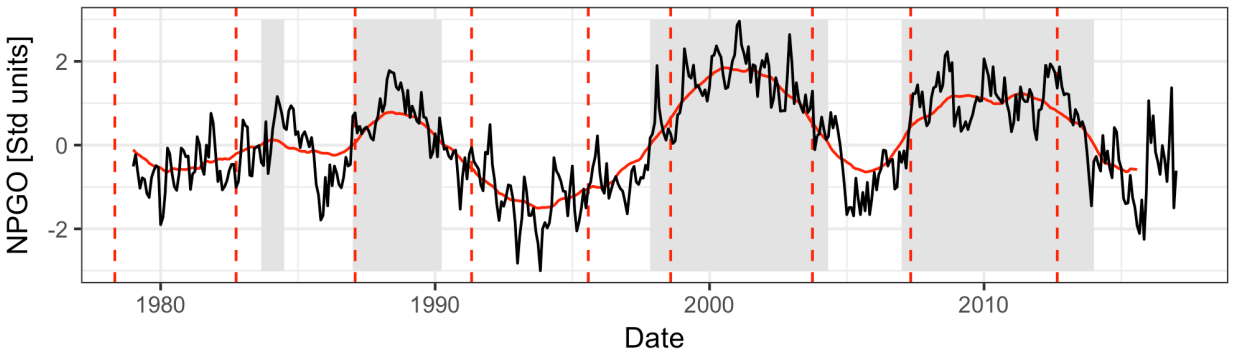

Supplementary Fig. 8: The North Pacific Gyre Oscillation (NPGO) index plotted for the interval of the CalCOFI Si_{ex} dataset. The black line plots raw index values, while the red line plots a three-year rolling mean of the inex. Shaded regions highlight durations when the NPGO rolling mean is positive. Red dashed lines indicate times where Nonparametric Multiple Change Point Analysis [65] indicated a significant distributional change of the NPGO rolling mean. Change point analysis roughly partitions the periods of positive and negative NPGO index values.

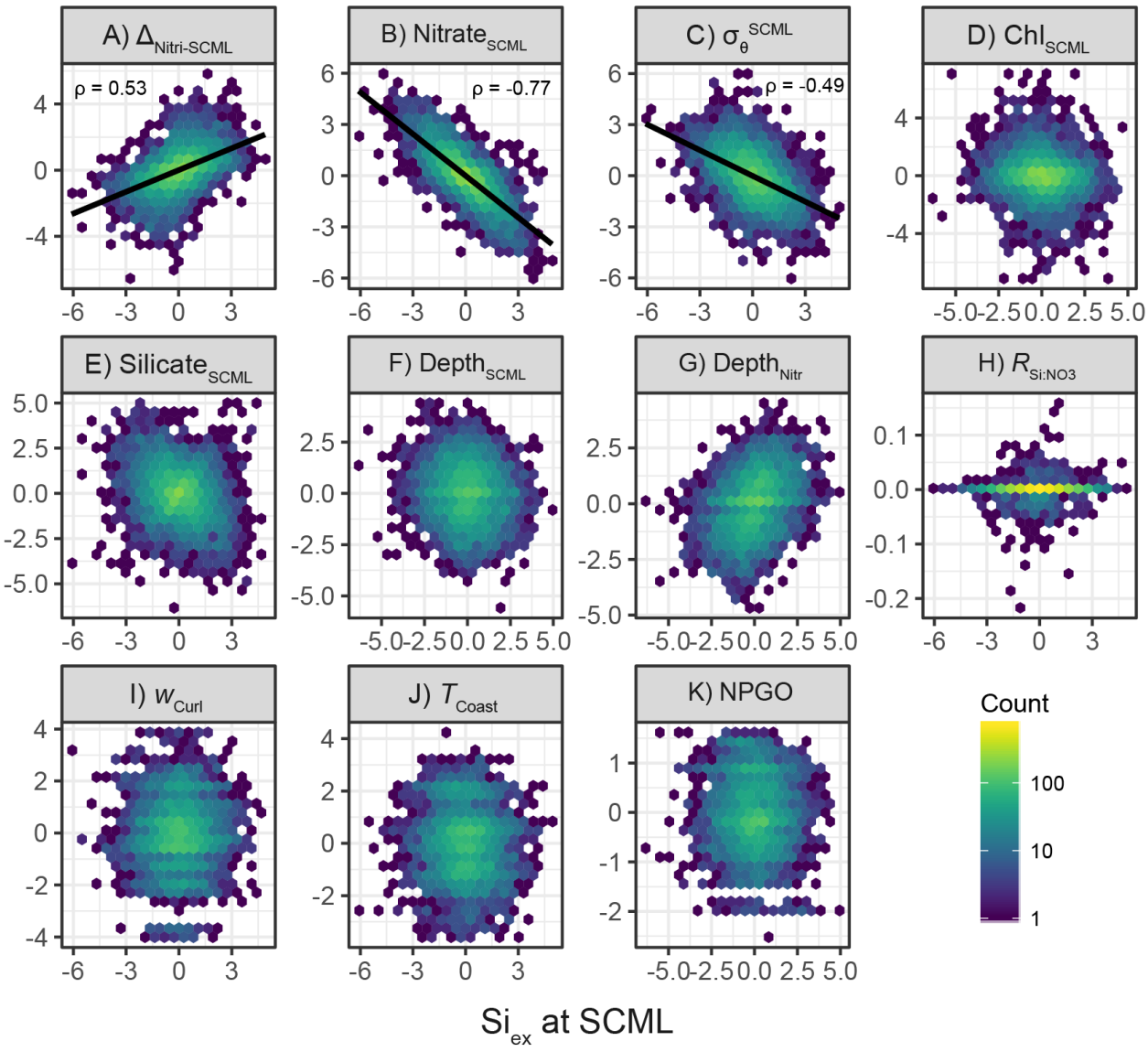

Supplementary Fig. 9: Relationships between SCML Si_{ex} values (horizontal axis) and other biogeochemical/hydrographic/physical transport parameters (vertical axis). Each hexagonal bin depicts a spatial histogram on x-y grid and the color of each bin is proportional to the number of data points within that gridded area. All time series were scaled to a mean of zero and standard deviation of one, then differenced by a time lag of one month to remove temporal autocorrelations (as assessed through an Augmented Dickey–Fuller test as well as the Kwiatkowski-Phillips-Schmidt-Shin (KPSS) test). Pearson product-moment correlation coefficients exceeding |0.4| are displayed in each plot. All correlations have a false discovery rate corrected $P <<< 0.05$. A) Difference in depth (meters) between the nitracline (defined by a threshold concentration of 1 μmol NO_3 L^{-1} and the SCML. Negative values indicate a shallower nitracline than the SCML. B) NO_3 concentrations at the SCML. C) Potential density at the SCML. D) Chlorophyll *a* concentrations at the SCML. E) Silicate concentrations at the SCML. F) Depth of the SCML. G) Nitracline depth. H) $R_{Si:NO3}$ ratio from the σ_θ = 26.5 kg m^{-3} density surface. I) Vertical velocity of curl-driven upwelling at the base of the mixed layer at 33° N 119° W J) Ekman driven coastal upwelling measured at 33° N 119° W K) North Pacific Gyre Oscillation

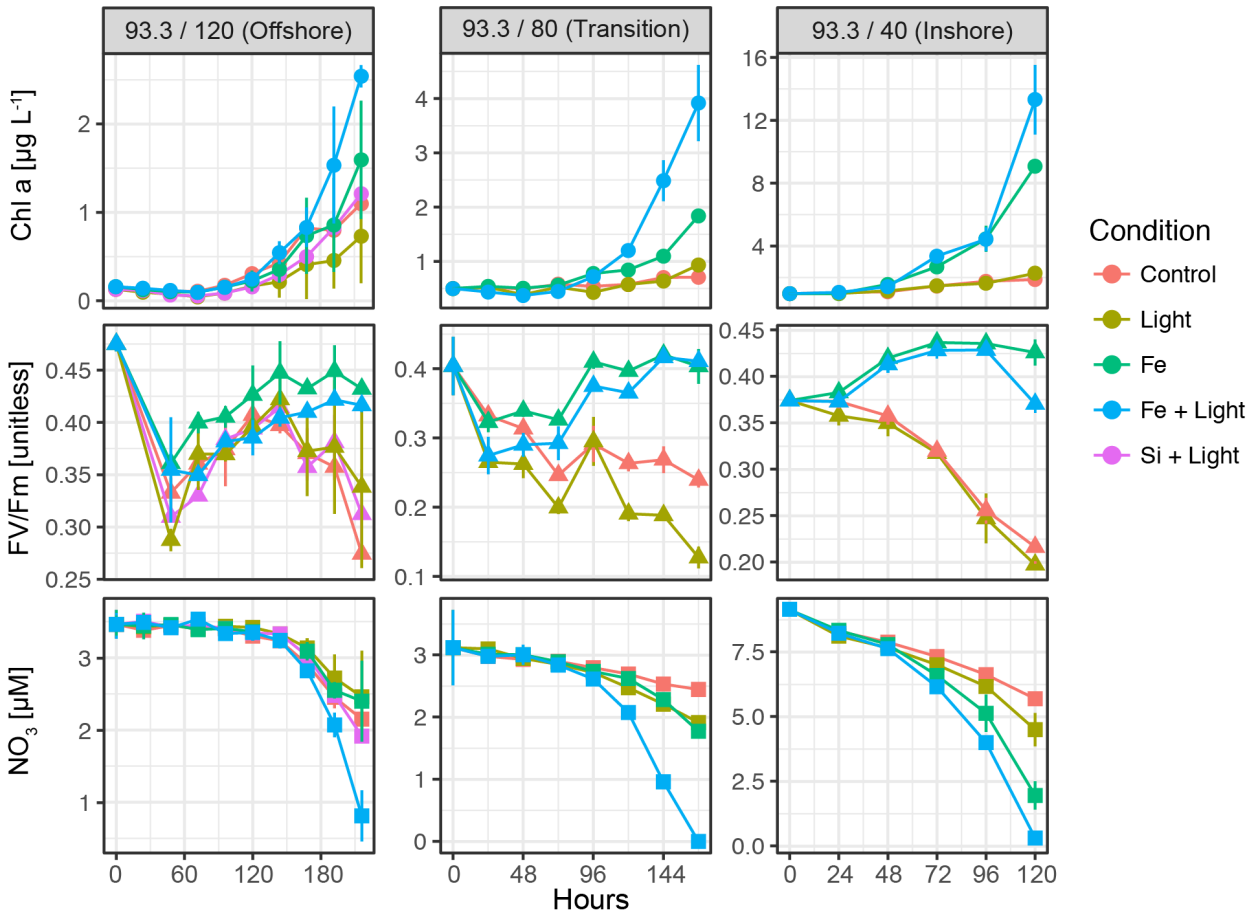

Supplementary Fig 10: Time course of chlorophyll *a* concentrations [µg L-1], maximum quantum yield of photosystem II [Fv/Fm], and nitrate concentrations [µg L-1] from incubation experiments conducted at stations 93.3/40, 93.3/80, and 93.3/120 during the DCM07 cruise. Points represent means of replicate incubations and error bars represent standard deviations of duplicate or triplicate samples.

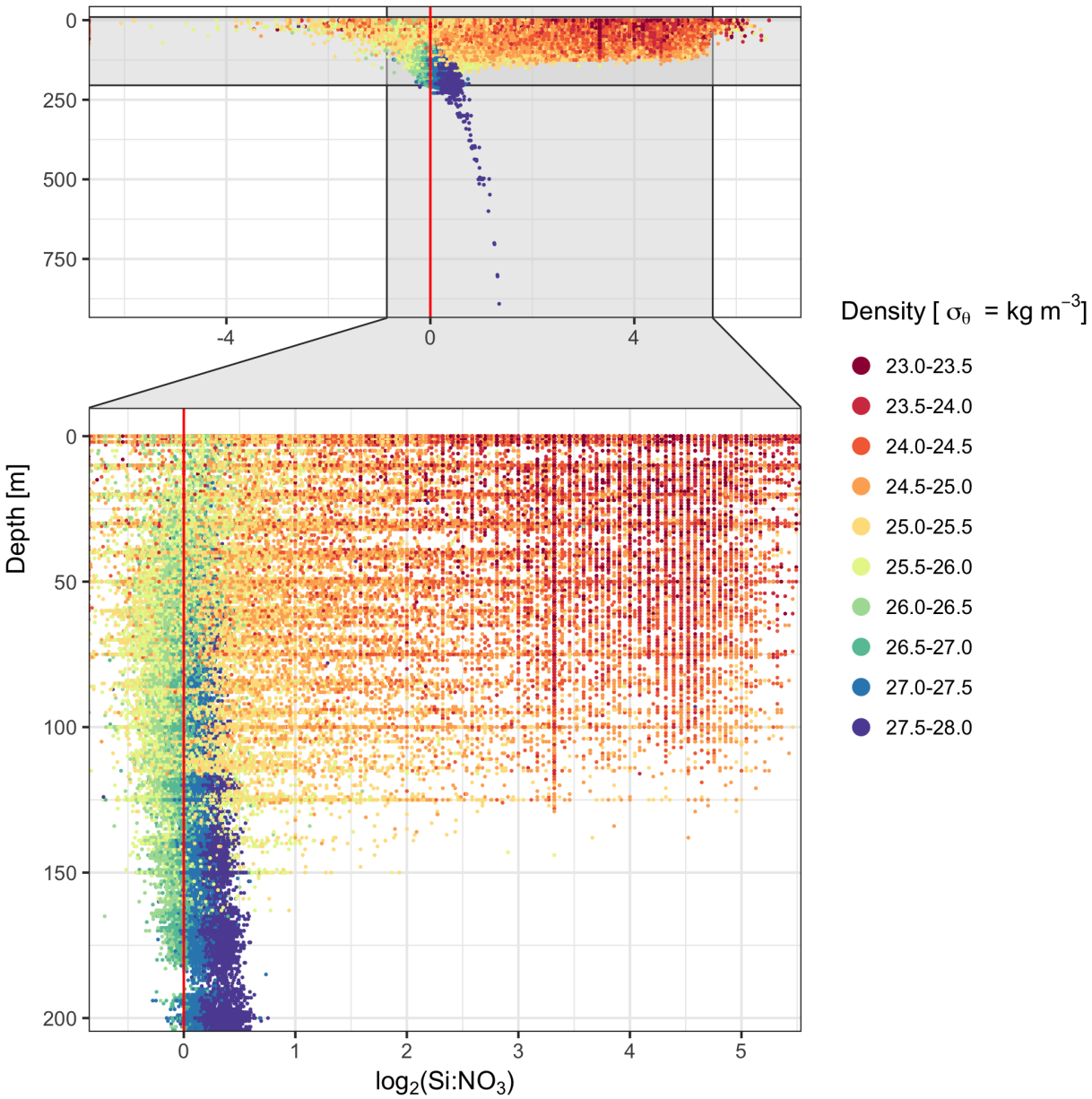

Supplementary Fig. 11: Log_2 transformed $Si:NO_3$ ratio vs depth for the entire CalCOFI dataset (1978-2017). Each point represents a discrete sample and color indicates potential density anomaly at each depth (σ_θ = kg m^{-3}) binned by 0.5 increments. Bottom inset is a zoomed perspective of the top.

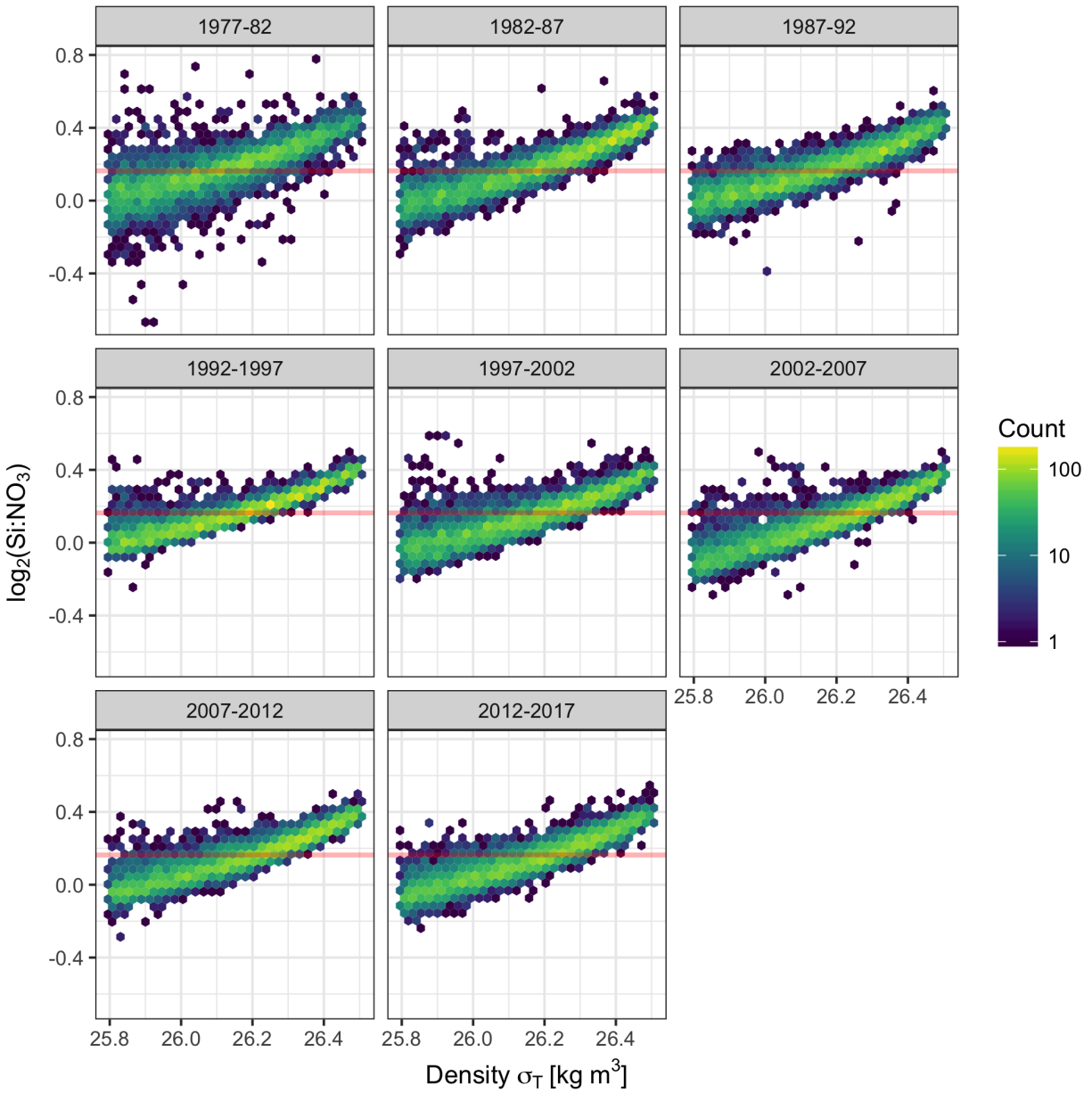

552
553
554 **Supplementary Fig. 12:** Log_2 transformed $Si:NO_3$ ratio vs potential density anomaly (σ_θ = kg m^{-3}) for the
555 entire CalCOFI dataset (1978-2017) binned by 5-year intervals. Each hexagonal bin depicts a spatial
556 histogram on the $Log_2(Si:NO_3)$ vs potential density grid and the color of each bin is proportional to the
557 number of samples within that gridded area. Color scale has been Log_{10} transformed. Red horizontal lines
558 represent the mean $Si:NO_3$ ratio for the entire temporally/spatially combined CalCOFI dataset.
559
560
561

562
563
564
565

Supplementary References:

49. Buck, K. N., Sohst, B. & Sedwick, P. N. The organic complexation of dissolved iron along the U.S. GEOTRACES (GA03) North Atlantic Section. *Deep Sea Res. Part 2 Top. Stud. Oceanogr.* **116,** 152–165 (2015).
50. Rue, E. L. & Bruland, K. W. Complexation of iron(III) by natural organic ligands in the Central North Pacific as determined by a new competitive ligand equilibration/adsorptive cathodic stripping voltammetric method. *Mar. Chem.* **50,** 117–138 (1995).
51. Buck, K. N., Lohan, M. C., Berger, C. J. M. & Bruland, K. W. Dissolved iron speciation in two distinct river plumes and an estuary: Implications for riverine iron supply. *Limnol. Oceanogr.* **52,** 843–855 (2007).
52. Stewart, F. J., Ottesen, E. A. & DeLong, E. F. Development and quantitative analyses of a universal rRNA-subtraction protocol for microbial metatranscriptomics. *ISME J.* **4,** 896–907 (2010).
53. Rho, M., Tang, H. & Ye, Y. FragGeneScan: predicting genes in short and error-prone reads. *Nucleic Acids Res.* **38,** e191 (2010).
54. Quast, C. *et al.* The SILVA ribosomal RNA gene database project: improved data processing and web-based tools. *Nucleic Acids Res.* **41,** D590–6 (2013).
55. Niu, B., Fu, L., Sun, S. & Li, W. Artificial and natural duplicates in pyrosequencing reads of metagenomic data. *BMC Bioinformatics* **11,** 187 (2010).
56. Morgulis, A. *et al.* Database indexing for production MegaBLAST searches. *Bioinformatics* **24,** 1757–1764 (2008).
57. Markowitz, V. M. *et al.* IMG: the Integrated Microbial Genomes database and comparative analysis system. *Nucleic Acids Res.* **40,** D115–22 (2012).
58. Kanehisa, M. *et al.* Data, information, knowledge and principle: back to metabolism in KEGG. *Nucleic Acids Res.* **42,** D199–205 (2014).

59. Benson, D. A. *et al.* GenBank. *Nucleic Acids Res.* **40,** D48–53 (2012).
60. Kersey, P. J. *et al.* Ensembl Genomes 2016: more genomes, more complexity. *Nucleic Acids Res.* **44,** D574–80 (2016).
61. Zeigler Allen, L. *et al.* The Baltic Sea Virome: Diversity and Transcriptional Activity of DNA and RNA Viruses. *mSystems* **2,** (2017).
62. Matsumoto, K., Sarmiento, J. L. & Brzezinski, M. A. Silicic acid leakage from the Southern Ocean: A possible explanation for glacial atmospheric pCO2. *Global Biogeochem. Cycles* **16,** 5–1–5–23 (2002).
63. Bograd, S. J. *et al.* Changes in source waters to the Southern California Bight. *Deep Sea Res. Part 2 Top. Stud. Oceanogr.* **112,** 42–52 (2015).
64. Pozo Buil, M. & Di Lorenzo, E. Decadal dynamics and predictability of oxygen and subsurface tracers in the California Current System. *Geophys. Res. Lett.* **44,** 2017GL072931 (2017).
65. James, N. & Matteson, D. ecp: An R Package for Nonparametric Multiple Change Point Analysis of Multivariate Data. *Journal of Statistical Software, Articles* **62,** 1–25 (2015).
66. Ohman, M. *et al.* Ecological Transitions in a Coastal Upwelling Ecosystem. *Oceanography* **26,** 210–220 (2013).
67. Di Lorenzo, E. Seasonal dynamics of the surface circulation in the Southern California Current System. *Deep Sea Res. Part 2 Top. Stud. Oceanogr.* **50,** 2371–2388 (2003).
68. Moore, C. M. *et al.* Processes and patterns of oceanic nutrient limitation. *Nat. Geosci.* **6,** 701–710 (2013).
69. Saito, M. A., Goepfert, T. J. & Ritt, J. T. Some thoughts on the concept of colimitation: Three definitions and the importance of bioavailability. *Limnol. Oceanogr.* **53,** 276–290 (2008).
70. Boyd, P. W. *et al.* Mesoscale Iron Enrichment Experiments 1993-2005: Synthesis and Future Directions. *Science* **315,** 612–617 (2007).

71. Gleeson, S. K. & Tilman, D. Plant Allocation and the Multiple Limitation Hypothesis. *Am. Nat.* **139,** 1322–1343 (1992).
72. Arrigo, K. R. Marine microorganisms and global nutrient cycles. *Nature* **437,** 349–355 (2005).
73. Brzezinski, M. A. The Si:C:N ratio of marine diatoms: Interspecific variability and the effect of some environmental variables. *J. Phycol.* **21,** 347–357 (1985).
74. Takeda, S. Influence of iron availability on nutrient consumption ratio of diatoms in oceanic waters. *Nature* **393,** 774–777 (1998).
75. M. Franck, V., Brzezinski, M. A., Coale, K. H. & Nelson, D. M. Iron and silicic acid concentrations regulate Si uptake north and south of the Polar Frontal Zone in the Pacific Sector of the Southern Ocean. *Deep Sea Res. Part 2 Top. Stud. Oceanogr.* **47,** 3315–3338 (2000).
76. Lynn, R. J. & Simpson, J. J. The California Current system: The seasonal variability of its physical characteristics. *J. Geophys. Res.* **92,** 12947–12966 (1987).
77. Bograd, S. J. & Lynn, R. J. Long-term variability in the Southern California Current System. *Deep Sea Res. Part 2 Top. Stud. Oceanogr.* **50,** 2355–2370 (2003).
78. de Verneil, A. & Franks, P. J. S. A pseudo-Lagrangian method for remapping ocean biogeochemical tracer data: Calculation of net Chl-a growth rates: PSEUDO-LAGRANGIAN GROWTH RATES. *J. Geophys. Res. C: Oceans* **120,** 4962–4979 (2015).
79. Boyd, P. W., Ellwood, M. J., Tagliabue, A. & Twining, B. S. Biotic and abiotic retention, recycling and remineralization of metals in the ocean. *Nat. Geosci.* **10,** 167–173 (2017/03//print).
80. Wan, X. S. *et al.* Ambient nitrate switches the ammonium consumption pathway in the euphotic ocean. *Nat. Commun.* **9,** 915 (2018).
81. Santoro, A. E., Casciotti, K. L. & Francis, C. A. Activity, abundance and diversity of nitrifying archaea and bacteria in the central California Current. *Environ. Microbiol.* **12,**

644 1989–2006 (2010).
645 82. Smith, J. M., Damashek, J., Chavez, F. P. & Francis, C. A. Factors influencing nitrification
646 rates and the abundance and transcriptional activity of ammonia-oxidizing microorganisms
647 in the dark northeast Pacific Ocean: Nitrification and AOA in the Dark Ocean. *Limnol.*
648 *Oceanogr.* **61,** 596–609 (2016).
649 83. Santoro, A. E. *et al.* Measurements of nitrite production in and around the primary nitrite
650 maximum in the central California Current. *Biogeosciences* **10,** 7395–7410 (2013).
651 84. Messié, M. *et al.* Potential new production estimates in four eastern boundary upwelling
652 ecosystems. *Prog. Oceanogr.* **83,** 151–158 (2009).
653 85. Messié, M. & Chavez, F. P. Nutrient supply, surface currents, and plankton dynamics
654 predict zooplankton hotspots in coastal upwelling systems: Biological Hotspots in Upwelling
655 Systems. *Geophys. Res. Lett.* **44,** 8979–8986 (2017).

656